NTNU
Det skapende universitet

CFD-analyse av en høytrykks Francis turbin

Anders Linde Holo

Master i produktutvikling og produksjon
Oppgaven levert: Desember 2011
Hovedveileder: Ole Gunnar Dahlhaug, EPT

Norges teknisk-naturvitenskapelige universitet

NTNU
Norges teknisk-naturvitenskapelige universitet

Institutt for energi- og prosessteknikk

EPT-M-2011-101

MASTEROPPGAVE

for

Stud.techn. Anders Linde Holo
Høsten 2011

CFD-analyse av en høytrykks Francis turbin
CFD-analysis of a high head Francis turbine

Bakgrunn og målsetting

Norske turbiner opererer på meget varierende last i tider med varierende pris og vannivå i magasinene. Det er en kjent at man får økte utmattingskrefter når turbinene opererer på fullast eller dellast. Ved dellast er turbinene påvirket av utmattingskrefter fra trykkpulsasjoner som blant annet er initiert av strømningen i sugerøret. Denne sugerør-strømningen er påført fra løpehjulet og inneholder flere spesielle fenomener som for eksempel "sugerørsvirvelen" og "vortex breakdown". Det er først og fremst den roterende strømningen som skaper disse fenomenene og fysikken i dette er ennå ikke fullt ut forstått. Dette arbeidet vil være en fortsettelse av arbeidet som Simen Breivik gjennomførte i sin masteroppgave våren 2011.

Mål

Utarbeide 3D-tegning og gjennomføre FSI-analyse av ledeapparat og løpehjul i en Francis turbin.

Oppgaven bearbeides ut fra følgende punkter

1. Litteratursøk
   a. Finne relevante publikasjoner der det er gjennomført CFD-analyse av løpehjul og sugerør i Francis turbiner
2. Studenten skal gjøre seg kjent med følgende:
   a. Modell test av Francis turbin fra Tokke Kraftverk
   b. Trykkmålinger på modellturbin gjennomført av Einar Kobro i sitt PhD-arbeid
3. Software kunnskap:
   a. Gjøre seg kjent med CFD-analyse vha CFX
   b. Gjøre seg kjent med FSI vha Ansys
   c. Gjøre seg kjent med DAK programmet Pro-Engineer
4. Utarbeide komplett 3D-tegning av modellturbinen fra Tokke Kraftverk
5. Lage et CFD- og FEM-grid av ledeapparat og løpehjul for Francis turbinen ved Tokke Kraftverk
6. Gjennomføre FSI-analyse av løpehjul til Tokke Kraftverk på beste driftspunkt for å se på innflytelsen av trykkpulsasjonene fra ledeskovlene på spenningene i bladene i turbinen. Dette gjennomføres på modell turbin.
7. Dersom det er tid så skal studenten sammenligne FSI-analysen med modelltester fra Vannkraftlaboratoriet.

Senest 14 dager etter utlevering av oppgaven skal kandidaten levere/sende instituttet en detaljert fremdrift- og eventuelt forsøksplan for oppgaven til evaluering og eventuelt diskusjon med faglig ansvarlig/veiledere. Detaljer ved eventuell utførelse av dataprogrammer skal avtales nærmere i samråd med faglig ansvarlig.

Besvarelsen redigeres mest mulig som en forskningsrapport med et sammendrag både på norsk og engelsk, konklusjon, litteraturliste, innholdsfortegnelse etc. Ved utarbeidelsen av teksten skal kandidaten legge vekt på å gjøre teksten oversiktlig og velskrevet. Med henblikk på lesning av besvarelsen er det viktig at de nødvendige henvisninger for korresponderende steder i tekst, tabeller og figurer anføres på begge steder. Ved bedømmelsen legges det stor vekt på at resultatene er grundig bearbeidet, at de oppstilles tabellarisk og/eller grafisk på en oversiktlig måte, og at de er diskutert utførlig.

Alle benyttede kilder, også muntlige opplysninger, skal oppgis på fullstendig måte. For tidsskrifter og bøker oppgis forfatter, tittel, årgang, sidetall og eventuelt figurnummer.

Det forutsettes at kandidaten tar initiativ til og holder nødvendig kontakt med faglærer og veileder(e). Kandidaten skal rette seg etter de reglementer og retningslinjer som gjelder ved alle (andre) fagmiljøer som kandidaten har kontakt med gjennom sin utførelse av oppgaven, samt etter eventuelle pålegg fra Institutt for energi- og prosessteknikk.

Risikovurdering av kandidatens arbeid skal gjennomføres i henhold til instituttets prosedyrer. Risikovurderingen skal dokumenteres og inngå som del av besvarelsen. Hendelser relatert til kandidatens arbeid med uheldig innvirkning på helse, miljø eller sikkerhet, skal dokumenteres og inngå som en del av besvarelsen.

I henhold til "Utfyllende regler til studieforskriften for teknologistudiet/sivilingeniørstudiet" ved NTNU § 20, forbeholder instituttet seg retten til å benytte alle resultater og data til undervisnings- og forskningsformål, samt til fremtidige publikasjoner.

Besvarelsen leveres digitalt i DAIM. Et faglig sammendrag med oppgavens tittel, kandidatens navn, veileders navn, årstall, instituttnavn, og NTNUs logo og navn, leveres til instituttet som en separat pdf-fil. Etter avtale leveres besvarelse og evt. annet materiale til veileder i digitalt format.

NTNU, Institutt for energi- og prosessteknikk, 22. august 2011

Olav Bolland
Instituttleder

Ole Gunnar Dahlhaug
Faglig ansvarlig/veileder

Medveileder(e) Torbjørn K. Nielsen

Preface

This master thesis was written by Anders Linde Holo at The Waterpower Laboratory at The Norwegian University of Science and Technology, during the fall semester of 2011. The supervisor of this thesis is professor Ole Gunnar Dalhaug. The goal was to perform fluid structure interaction (FSI) simulations at the Tokke model runner at best efficiency point (BEP), and compare the results with laboratory measurements.

I would like to thank my supervisor Ole Gunnar Dahlhaug who has been supportive throughout this work and provided helpful information, and Norconsult, by Andre Reyould and Halvard Bjørndal, who came up with the idea for this thesis, and also have been supportive.

I will also thank Simen Breivik, Mette Eltvik, Martin Aasved Holst, Peter Joakim Gogstad and Kyrre Reintertsen for valuable help, discussions and advice, and all the people at the waterpower laboratory for great support and a joyful atmosphere throughout the semester.

Oslo, 30 December, 2011

Anders Holo

Abstract

In this thesis fluid structure interaction (FSI) simulations of the Tokke turbine model have been conducted at conditions reported to be best efficiency point (BEP) and compared to lab measurements. The simulations results show that the turbine operated slightly off BEP, and that simulation results are close to the laboratory measurement. The deviation in efficiency between FSI results and lab measurements is 5.2%. The deviation in net head between the lab measurements and the simulations is 0.2m, which corresponds to a mismatch of less than 1%. The deviations in net head and efficiency between simulation results and laboratory measurement results are small and therefore the simulation results are considered to be satisfactory.

In order study the pressure pulsations from the guide vanes primarily four steady state FSI simulations were conducted. For each simulation the runner was slightly rotated, whereas the wicket gate was fixed. This was done to cover a complete dynamic load cycle for the runner. Subsequently the stresses in two points, where high stress was seen, in the runner blade were studied for all four simulations. The highest dynamic stress peak to peak amplitude is 5.86Mpa, where the mean stress is 18.42Mpa. Hence the dynamic stress corresponds to 31.8% of the total stress. There is a difference in laboratory measured stress and the FSI calculated stress. The differences between the maximum stress of the laboratory measurements and simulations are probably due to the small differences in probe locations, but may also be a consequence of uncertainties in computational fluid dynamics (CFD) and finite element method (FEM) simulations and measuring uncertainty. However, the correlation is good, and would be even better if denser meshes could be applied, and if a greater load spectrum were studied. Computer power sat a limitation for the simulations.

Both the FSI simulations and the lab measurements show that dynamic stress corresponds to a big percentage of the total stress. Hence, in additions to existing parameters the energy companies should give operation plans in their specifications to the manufactures. The operations plans would give the turbine manufactures the necessary information so that dynamic loads can be accounted for in turbine design.

Sammendrag

I denne masteroppgaven har det blitt gjennomført «fluid structure interaction» (FSI) simuleringer av modellturbinen fra Tokke, ved innløpsbetingelser som var rapportert å gjelde ved best driftspunkt. Simuleringsresultatene ble sammenlignet med laboratoriemålinger. Simuleringsresultatene viser at turbinene opererte nære, men ikke helt på beste driftspunkt, og at simuleringsresultatene er nesten like laboratoriemålingene. Virkningsgradsavviket mellom simuleringsresultatene og laboratoriemålingene 5.2%. Avviket i trykkhøyde mellom simuleringsresultatene og laboratoriemålingene er 0.2m. Dette tilsvarer et avvik på mindre enn én prosent. Avviket i trykkhøyde og virkningsgrad mellom simuleringsresultatene og laboratoriemålingene er små og simuleringsresultatene er derfor vurdert til å være tilfredsstillende.

For å studere trykkpulsasjonene fra ledeskovlene, ble fire «steady state» FSI simuleringer gjennomført. For hver av simuleringene ble løpehjulet litt rotert i forhold til ledeapparatet. Dette ble gjort for å dekke en hel lastsyklus for løpehjulet. Deretter ble spenningen i to punkter i turbinbladet, som ble plassert i områder med stor spenning, studert for alle fire simuleringene. Den største dynamiske spenningen er 5.86Mpa, hvor den gjennomsnittlige spenningen er 18.42Mpa. Følgelig utgjør den dynamiske spenningen 31.8% av den totale spenningen. Det er liten forskjell i spenningsverdier mellom laboratoriemålingene og simuleringene. Forskjellene i maksimumsspenningene mellom simuleringsresultatene og lab-resultatene kan være på grunn av den lille forskjellen i målepunktlokasjonene, men også på grunnen av usikkerhet i «computational fluid dynamics» (CFD) og «finite element method» (FEM) simuleringene, men også måleusikkerhet. Likevel er det en sterk korrelasjon mellom simuleringer og laboratoriemålinger, og den ville blitt enda sterkere hvis finere mesh kunne blitt brukt, og et større lastområde ville blitt undersøkt. Mangel på datakraft var en begrensing for simuleringene.

Både FSI simuleringsresultatene og laboratoriemålingene viser at dynamiske spenninger utgjør en stor prosentandel av de totale spenningene. Derfor, i tillegg til foreliggende parametere, burde energiselskapene vise kjøreplanen i spesifikasjonene til turbinprodusentene. Kjøreplanen ville gitt turbinprodusentene den nødvendige informasjonen slik at det kunne bli tatt høyde for dynamiske laster i turbindesign.

Table of contents

Nomenclature

Symbol	Signification	Denomination
u^*	Shear velocity wall	[m/s]
y	Distance y to the wall	[m]
y^+	Dimensionless distance *y* to the wall	[-]
ν	Kinematic viscosity	[m^2/s]
p	pressure	[Pa]
$\vec{\omega}$	angular velocity vector	[1/s]
u^+	Dimensionless velocity parallel to the wall	[-]
u	velocity parallel to the wall	[m/s]
S_{ij}	Rate of deformation	[-]
Re	Reynolds number	[-]
Q	Mass flow	[m^3/s]
τ	Shear force	[Pa]
$\vec{f}$	Body forces vector	[m/s^2]
$\vec{g}$	gravity vector	[m/s^2]
ρ	Density	[kg/m^3]
k	Turbulent kinetic energy	[m^2/s^2]
$\vec{U}$	Velocity vector	[m/s]
U	Velocity magnitude	[m/s]
μ	Dynamic viscosity	[Ns/m^2]
μ_t	Turbulent viscosity	[Ns/m^2]
σ_κ	Turbulent model constant for the k – epsilon equation	[-]
P_k	Shear production of turbulence	[kg/ms^3]
β	Coefficient of thermal expansion	1/t

ω	Turbulent frequency	1/f
σ_ω	Turbulent model constant for the k – omega equation	[-]
α	Symbol used as a subscript to indicate that the quantity applies to phase α	[-]
β	Symbol used as a subscript to indicate that the quantity applies to phase β	[-]
ϵ	Turbulent dissipation	[m^2/s^3]
B_1	Inlet hight	[m]
r_0	Vanless space radius	[m]
r_1	Inlet runner radius	[m]
$\vec{F}$	Force vector	[N]
$\vec{M}$	Moment vector	[Nm]
$\vec{R}$	Radial direction vector	[-]
$\dot{m}$	Mass flow	[kgm^3/s]
E	Specific energy	[J]
η_h	Hydraulic efficiency	[-]
g	Gravity constant	[m/s^2]
H	Pressure height	[m]

Indexes

Index	Signification
ref	Reference
tot	Total
p	pipe
x	x- direction
y	y- direction
z	z- direction
w	wall

Abbreviations

CFD	Computational Fluid Dynamics
FEM	Finite Element Method
FSI	Fluid Structure Interaction
NTNU	Norwegian University of Science and Technology
BEP	Best Efficiency Point

Figure and Table list

Chapter 1: Introduction

An increasing number of failures have been detected in Francis runners shortly after they have been put into operation (1). Turbine manufactures have an increasing desire to cut fabrication costs and increase the runner efficiency, and energy companies have changed the operation schedule in order to maximize profit. Together these actions have been unfavorable to the robustness of Francis runners. The development has proceeded even though the material strength of the runners has remained unchanged.

The reason for the failures is fatigue at the trailing edge of the runner blades where the blades are thinner. These areas are heavily exposed to several sources of dynamic loading which, comprise rotor stator interaction, cavitation, draft tube surge, von Karman shredding and instabilities in the runner channels.

In this thesis, one potential cause to turbine cracking, the wake from guide vanes which causes pressure pulsations to propagate down the runner channels has been studied. That wake has been studied at best efficiency point (BEP) by use of computational fluid dynamics (CFD). Subsequently fluid structure interaction (FSI) simulations have been conducted to quantify the impact from the pressure pulsations on the runner blades. Finally, the results have been compared to lab measurements for verification.

Parts of this work have been published in the paper “Mechanical robustness of Francis runners, requirements to reduce the risk of cracks in blades” (1). The paper is presented in Appendix E.

In consultation with supervisor Ole Gunnar Dahlhaug it was decided that the focus for this Master thesis was to perform a Fluid Structure Interaction (FSI) analysis for the Tokke turbine model runner.

Chapter 2: Background

When a new hydropower plant is built, a turbine has to be designed for the specific case. This means that extensive analyses have to be done when designing turbines. Laboratory tests and FSI analyses have been performed for several years at laboratories around the world, including NTNU. Some prior work that is relevant to this thesis is presented in 2.1.

2.1 Prior work

The author has performed simulation for the spiral casing for the Tokke turbine model (2). Some parts from that project were used in this thesis.

Kobro (3) conducted measurements at the Tokke model runner at the water power laboratory at NTNU. Pressure measurements were performed at both the pressure and suction side at a blade and splitter blade. The results are presented in 5.3. His work also presents several causes for pressure pulsations, e.g. the pressure pulsations from the wicket gate are due to rotor stator interaction. The pressure wake is considered to be steady in the wicket gate reference frame, but unsteadiness occurs in the runner reference frame. Together pressure pulsations are the effect of the pressure field from the guide vanes and the pressure field in the runner. The dynamic response decreases down the runner channels. By increasing the vaneless space the wake mixes out, but the vaneless space is often kept small due to construction costs.

Xiao et al. (4) performed FSI analysis, and concluded that the maximum Von Mises stresses in the runner are far below the materials yield stress, so the cracks are not caused by heavy static stresses, but by the combined effect of static- and dynamic stresses. Dynamic load at off best efficiency point is one of the main reasons for fatigue and cracks in runner blades.

Breivik (5) conducted CFD analyses of the runner and draft tube in the Tokke turbine model at the Waterpower Laboratory and compared the results to laboratory measurements. His draft tube- and runner mesh were used in this thesis as a basis for the meshes of the complete turbine system.

Antonsen (6) studied the impact of the wicket gate design on dynamic runner load. He concluded that guide vanes may be designed to decrease dynamic loads without compromising turbine efficiency. He also concluded that the guide vane wake matches well with classical wake theory, although the wake seems to mix out faster due to accelerated flow field. To verify the laboratory measurements he conducted, CFD was used. The comparison shows a deviation of 25% for 2D simulations and 15% for 3D simulations. This was considered to be satisfactory.

Nennemann et al. (7) studied the main problems occurring in a Francis turbine. CFD calculations were performed and compared to lab measurements. The results show that there

is a good match between CFD results and laboratory results. The work resulted in a new standard for conducting CFD analyses for turbines at GE Hydro.

2.2Ongoing work

At the Waterpower Laboratory some students are working on projects that are relevant to this thesis.

Jonas Bergmann- Paulsen is designing a turbine to which FSI analysis will be applied.

Peter Joachim Gogstad is working on making a retrofit design for a turbine at “La Higuera” hydropower plant in Chile. He is performing CFD analysis of the turbine. Subsequently the results will be applied to a FEM model in order to verify the integrity of the turbine.

Chapter 3: Applied Software

3.1ANSYS

ANSYS is a platform with several different programs especially designed to solve complex engineering challenges. The programs that have been used in this thesis are presented below.

3.1.1Workbench

Workbench, a recent invention by ANSYS, presents graphically an overall view of the project. Within Workbench subprojects can be created. To connect subprojects, one may use drag and drop or import existing results. Workbench supports parametric variations. This means that, e.g. a turbine can be tested at a wide range of design points by specifying boundary parameters. Unfortunately Workbench does not provide all the options as of stand-alone systems, especially multi- domain simulations often require the use of stand-alone systems. However, workbench works fine for basic cases.

3.1.2 Design Modeler

ANSYS contains a basic CAD tool named Design Modeler. To have Design Modeler skills is important when using ANSYS. If geometries are imported to ANSYS, very often these geometries need minor adjustments before simulation can be run. Geometries can also be made directly in Design Modeler, but the program is not as advanced as e.g. Autodesk Inventor.

3.1.3Mechanical APDL

It is now possible to solve problems without having competence of APDL which is the programming language in ANSYS. The scroll- down menus provides great opportunities, yet the menu based ANSYS does not include all the possibilities which APDL provides. By knowing the “language behind the shell” the programmer enhances the opportunity of getting preferable setups.

3.1.4 Mechanical

Static structural analysis can be conducted in Mechanical. A static structural analysis contains algorithms for solving both linear and nonlinear deformations. Except creating a model, everything can be done in Mechanical. This comprises, meshing, running simulations and evaluating results. In Mechanical all options can be selected from scroll- down menus. The meshing procedure is the same as of ANSYS Meshing which is described in 3.1.5.

3.1.5 ANSYS Meshing

ANSYS meshing is a program for making grids for CFD- and FEM purposes. Before constructing the mesh a model must be available. ANSYS meshing supports geometries made in Design Modeler or similar tools supported by ANSYS e.g. Autodesk Inventor.

The program contains various methods for controlling mesh resolution. To control the cell size one may specify maximum and minimum cell sizes. This can be done for the entire geometry or different sectors may be individually treated. To create inflation layers one may specify the size the inflations, such as First Layer Thickness, Total Thickness and Expansion Factor.

When starting to mesh one may experience difficulties concerning small faces. At the edge of each face ANSYS meshing creates finer meshes. The edges of the face may be at places where finer mesh is unnecessary. The program provides an option for merging these faces, called virtual topology. By doing this the mesh density may be lowered in areas where a dense mesh is not a necessity. Virtual faces can be created automatically and manually.

3.1.6 ICEM CFD

ICEM CFD is a program which gives the designer great meshing control. Meshes can be created both manually and automatically. The automatic option may give satisfactory meshes for a lot of cases, but is preferable to create meshes manually. Manual meshes can e.g. be created by specifying the nodal distribution at edges.

3.1.7 CFX- Pre

CFX Pre is the program where the conditions for the simulations are set. CFX Pre contains a turbo mode which can be used when dealing with turbo machinery. However, setting up the simulations manually gives the programmer greater control. The program also lets you choose how simulations are to be run e.g. how many partitions are dedicated for the run, memory allocated, and whether the simulations should be commissioned from initial conditions or current state simulations.

3.1.8CFX- Solver Manager

This program also lets you choose how simulations are to be run. When the simulations have begun, various parameters can be monitored.

3.1.9 CFD- Post

This is from where results are extracted. The program lets the user review results visually and graphically, and different parameters can be studied. CFD-Post produces standard reports

which can be of great convenience. However, these reports may contain more information than what is necessary. The user may also create tailor- made reports.

3.2 Autodesk Inventor

In consultation with supervisor Ole Gunnar Dahlhaug it was decided that the turbine was to be created in Autodesk Inventor.

Autodesk Inventor is CAD application which supports both 2D and 3D drawings, and may export files to several CFD and FEM tools. In Autodesk Inventor almost all kinds of drawings can be made, but it does not support creation of dual curved surfaces.

Chapter 4: Grid Analysis

To make a proper mesh for the entire case, first the wicket gate mesh domain was optimized to time economize the process. Subsequently, the meshes were connected to run the complete case, involving guide vanes, runner and draft tube. The simulations were conducted with the mass flow and guide vane opening for BEP stated in (3).

4.1 Guide Vanes mesh

Several meshes were made to find the optimal grid. Initially, a coarse mesh was made to make sure a simulation could be commissioned. Subsequently inflation layers were introduced in order to account for boundary layers effect, and make the turbulence model work properly. The first layer height of the inflation layers is 0.5 mm, and in total 5 layers was used with a growth rate of 1.2. This was done to ensure the transition between the inflation elements and the first ordinary element, to be sufficiently smooth.

4.1.1 Setup

Table 5, found in Appendix A, shows the input values for the simulations. The simulations were conducted at BEP for the model runner. More information regarding setup input options is found in Appendix B.

4.1.2 Grid validation

In total 11 grids with increasing density were made in order to find a proper grid- independent mesh. Grid 1 corresponds to the coarser grid, whereas grid 11 corresponds to the denser grid. Figure 1 shows the total pressure difference between inlet and outlet for the wicket gate. Figure 2 and Figure 3 show the Y + values at the wicket gate walls and the guide vanes.

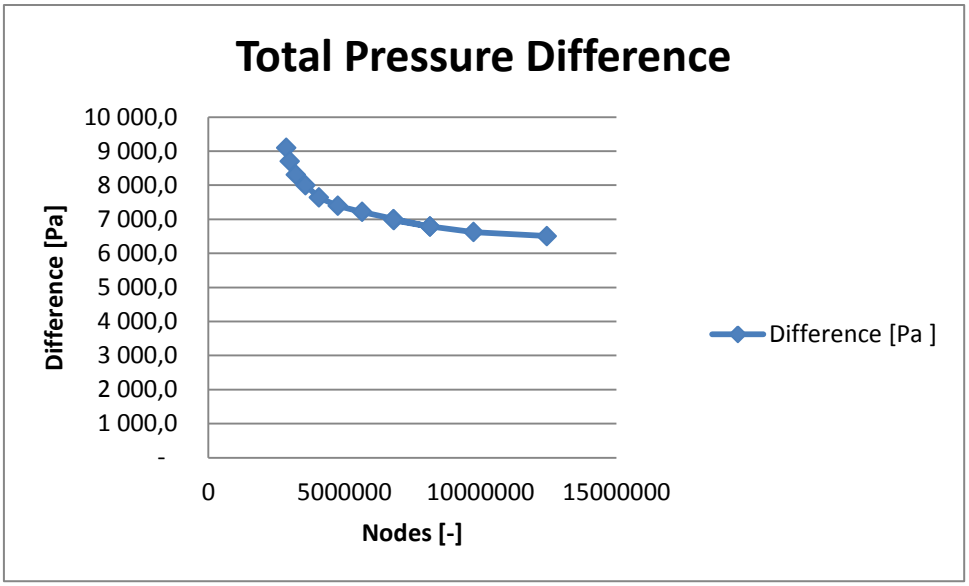

Figure 1: Total pressure difference

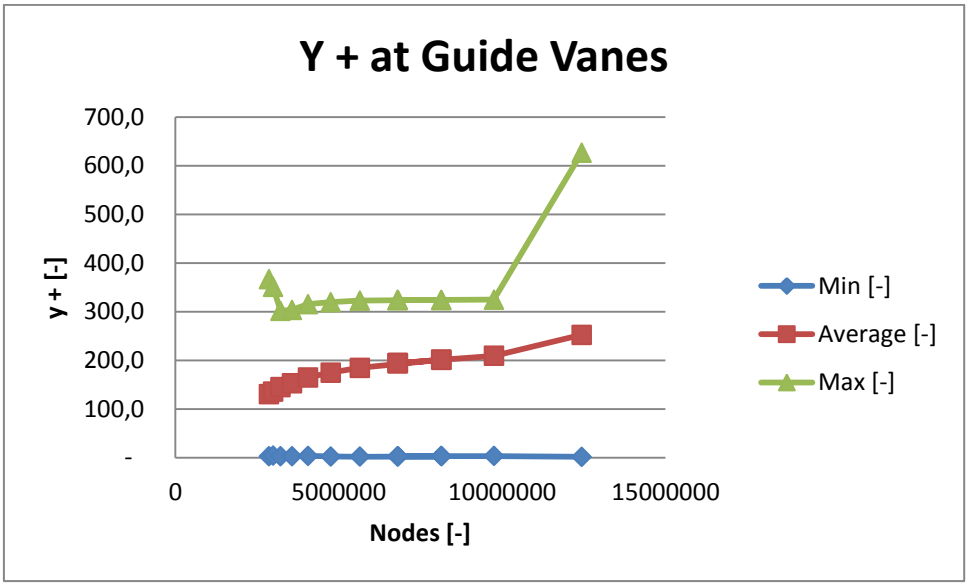

Figure 2: Y + at guide vanes

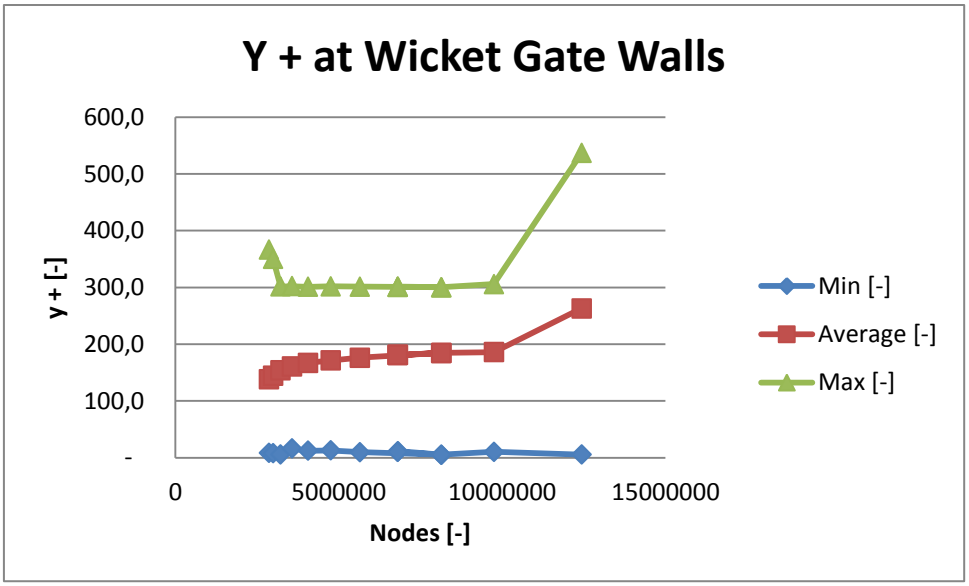

Figure 3: Y + at wicket gate walls

The deviation in pressure difference, ΔP between the last and second last simulation was calculated by the following formula:

$$Deviation[\%] = \frac{\Delta P_1 - \Delta P_2}{\Delta P_1} * 100 \qquad [1]$$

The deviation between grid 10- and grid 11- is 1.8%. The deviation approaches a converged solution. It would be preferable to run more simulations, but this was not done due to computer power limitations.

4.1.3Important flow features

This section shows important flow features for grid 10. Stagnation points of the guide vanes are shown in Figure 5, where the streamlines split. Y + values at the stagnation points are shown in Figure 4.

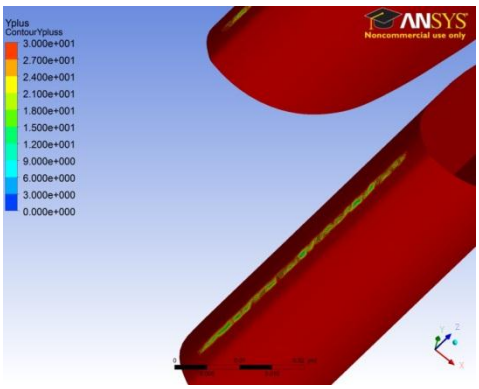

Figure 4: Y + at stagnation point

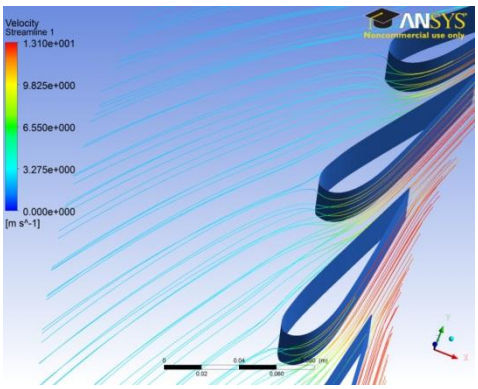

Figure 5: Velocity stream lines at guide vanes

The SST-turbulence model fails to calculate the turbulence in the surrounding areas of the stagnation points. This is within the area 2<Y+<30, where both the k-epsilon and k-omega

turbulence models are not valid. Figure 6 and Figure 7 shows the Y+ values at the rest of the guide vanes. Here, the Y + values are within the range for the k – epsilon turbulence model to work. More information about turbulence models is found in Appendix B.

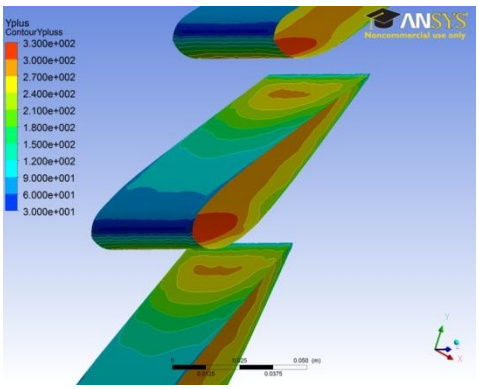

Figure 6: Y + at guide vanes 1

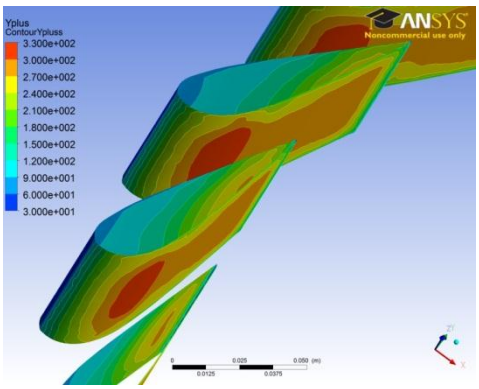

Figure 7: Y + at guide vanes 2

4.2CFD Merged Mesh; Guide Vanes, Runner and Draft tube

The building of the runner grid was originally initiated by Simen Breivik and further developed in this work. ICEM- CFD was used to create the mesh. The runner water path was divided into different blocks. The nodal distribution was set on the edges of the blocks, from which an unstructured hexagonal mesh was created.

In order to optimize the runner mesh, simulations were run until the Y + values were within satisfactory limits for most of the area. When trying to optimize the Y + values for the shroud and hub, negative volumes were created. Negative volumes are problematic to CFD, the solver fails to simulate negative volumes. Hence the solver could not start.

Attempts to refine the mesh were limited by computer memory. Adjusting the memory allocated for run ratio compensates for this, at the expense of simulation speed. This can be done up to a certain extent, and 1.2 is the higher recommended value (8). All simulations for the complete runner were conducted with this value.

Due to computer power limitations, a mesh with 1333500 nodes and 1218960 elements for the runner was used for the complete turbine run. The mesh is shown in Figure 8 and the mesh quality of the runner is shown in Figure 9. Higher values up to one at the x axis represent good quality. The y axis represents quantity of elements.

The reason for connecting the draft tube and the runner mesh was to obtain proper outlet conditions for the runner. Hence, the draft tube mesh was not optimized in this work.

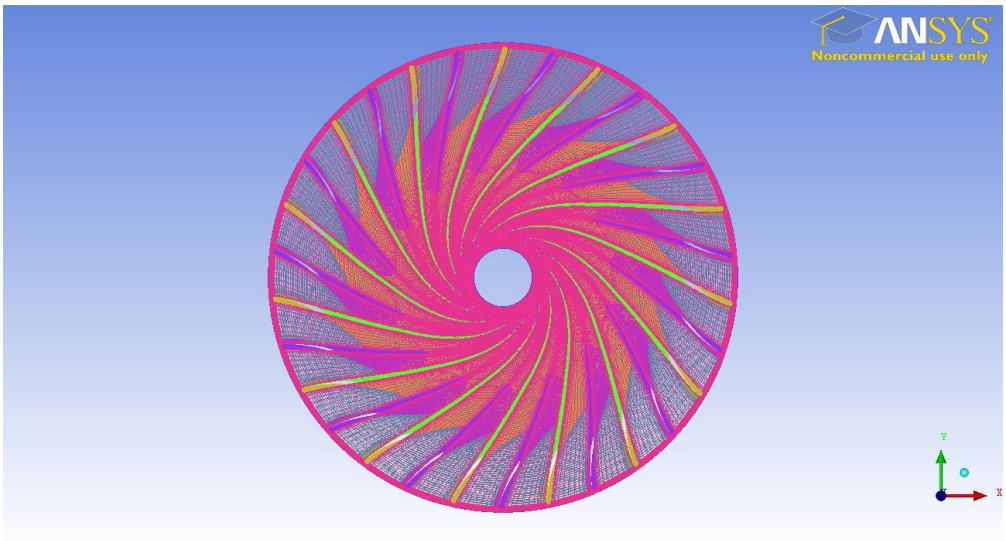

Figure 8: Runner mesh

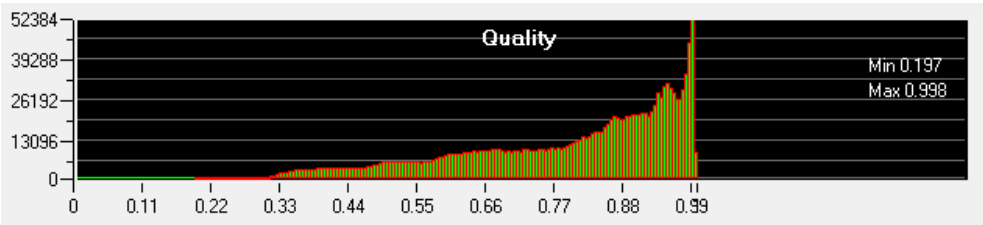

Figure 9: Quality of runner mesh

As simulations were to be conducted for the complete turbine, and the optimal mesh for the guide vanes consisted of ~ 10^7 elements, it would be preferable to use a mesh for one guide vane passage. This would have decreased the number of elements by a factor of 28, as the number of guide vanes are 28. This, however, was not feasible as the connection is two- way, and the flow in not uniform over the runner. As simulation could not run with denser meshes, a mesh with 2213600 elements for the guide vanes was used. This grid is further referred to as grid 12. This mesh was not originally part of the guide vane analysis, but had to be constructed in order to be able to run simulations. Figure 10 shows the quality of the wicket gate mesh.

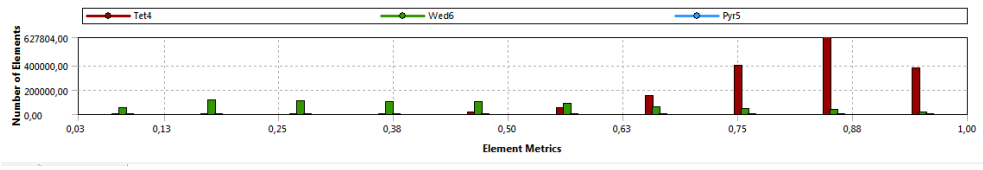

Figure 10: Quality of wicket gate mesh

Figure 11 shows grid 12. The mesh is denser around the guide vanes and inflations layers were used with the same setup as for grid 10.

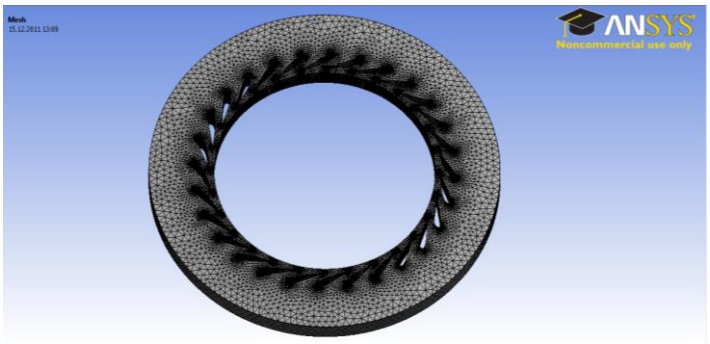

Figure 11: Wicket gate mesh

4.2.1Setup

Table 6, found in Appendix A, shows the input values for the complete turbine run. The mass flow and the guide vane opening is the same as for the model test at BEP.

4.2.2 Validation

The simulations show that the solutions converge well for both the wicket gate and the runner, whereas the parameters for the draft tube oscillate just above 10^{-4}. The grid in the draft tube was not optimized for this case, thus the results for the draft tube were disregarded. The parameter residuals are shown in Figure 12.

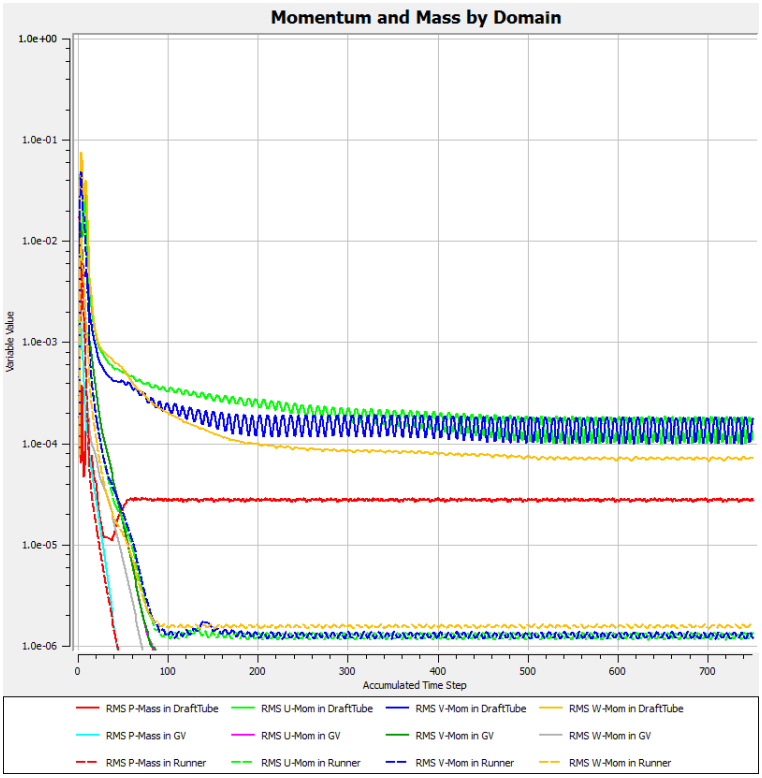

Figure 12: Parameter residuals for complete turbine run

4.2.3 Important flow features

This section presents important flow features for the complete turbine simulations.

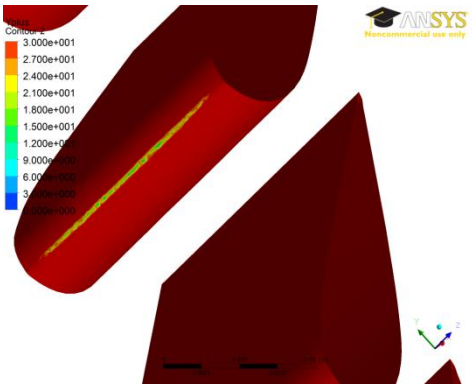

Figure 13: Y + at stagnation points

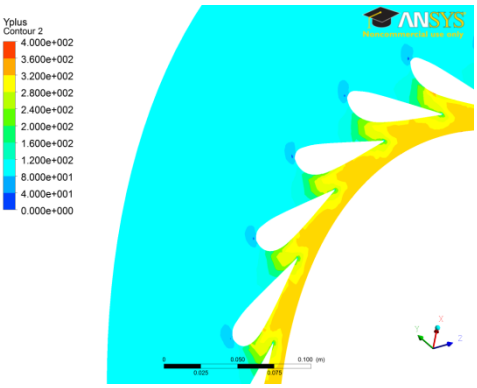

Figure 14: Y + at wicket gate walls

As explained in 4.1.3 grid 12 was used for the complete turbine simulations. This grid, as for grid 10, contains areas where the SST-turbulence model fails. This area is located at the stagnation point as shown in Figure 13. The stagnation point is also shown at the wicket gate wall in Figure 14. At the rest of the wicket gate wall the turbulence model works. Figure 15 and Figure 16 show the Y+ values at the guide vanes. Here the Y + values fall within the range in which the k- epsilon turbulence model is applicable.

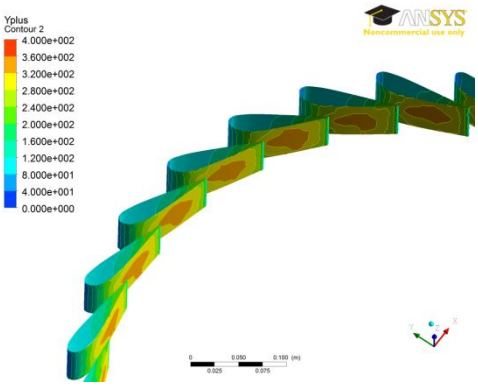

Figure 15: Y + at guide vanes 1

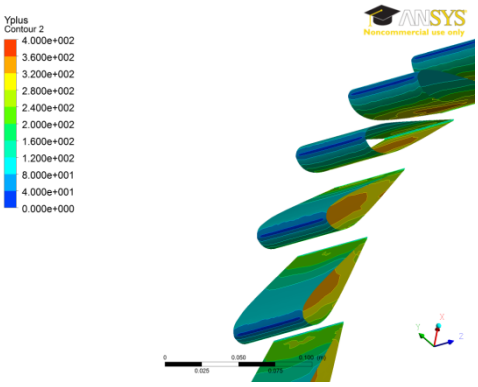

Figure 16: Y + at guide vanes 2

The streamlines at the runner outlet shown in Figure 17 and Figure 18 are not totally straight. The streamlines should be straight when operating at BEP. This indicates that the runner operates slightly off BEP.

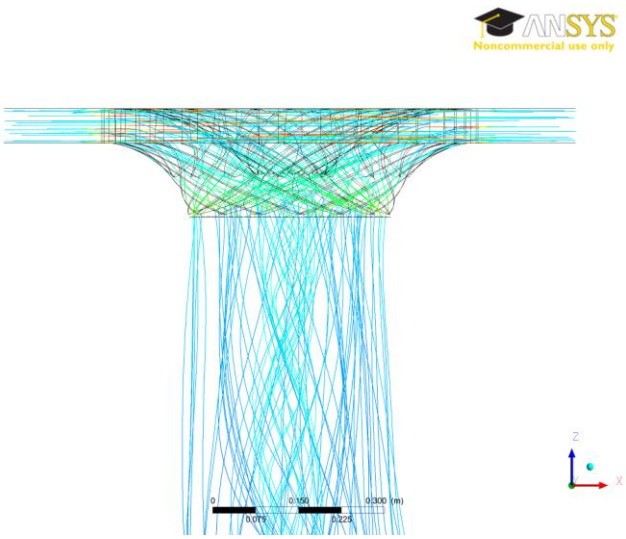

Figure 17: Draft tube velocity streamlines

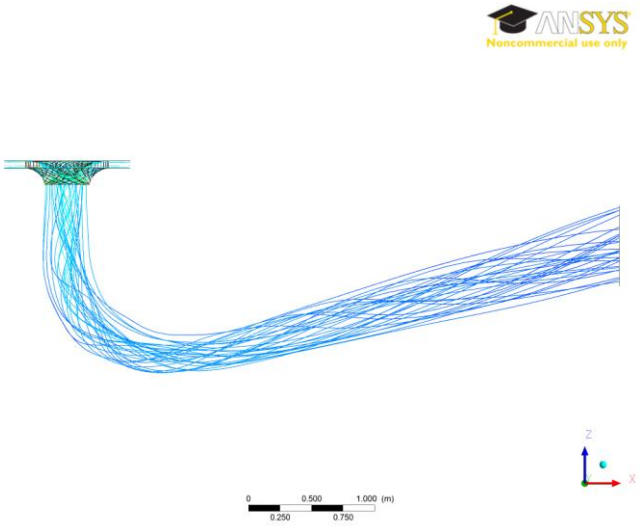

Figure 18: Full turbine velocity stream lines

Figure 19 shows the pressure distribution at the runner blades. The pressure is higher at the pressure side than at the suction side. This verifies that the simulations have been conducted in a correct way.

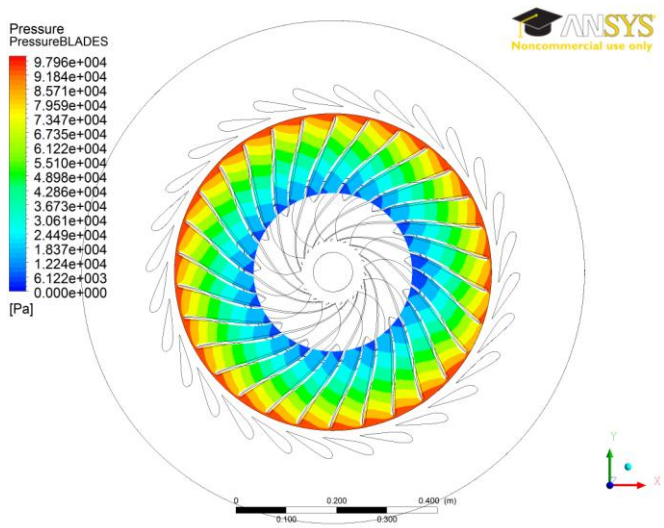

Figure 19: Pressure distribution in the runner

Figure 20 shows the streamlines at the guide vanes. Figure 21 shows that the water follows the runner blades. The streamlines also verifies that the simulations has been conducted in a correct way.

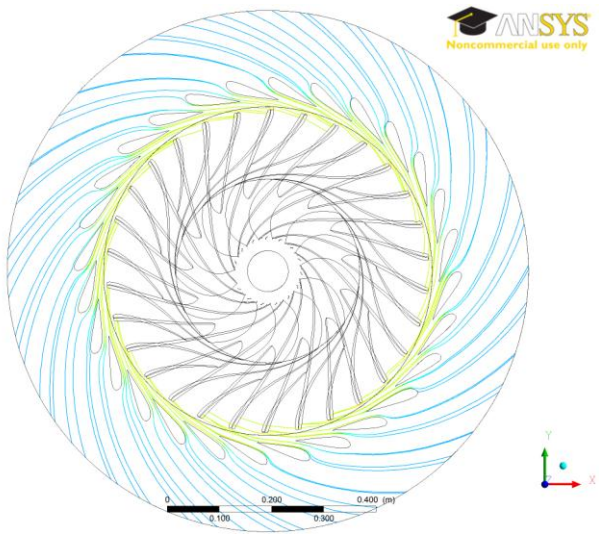

Figure 20: Stationary frame velocity streamlines

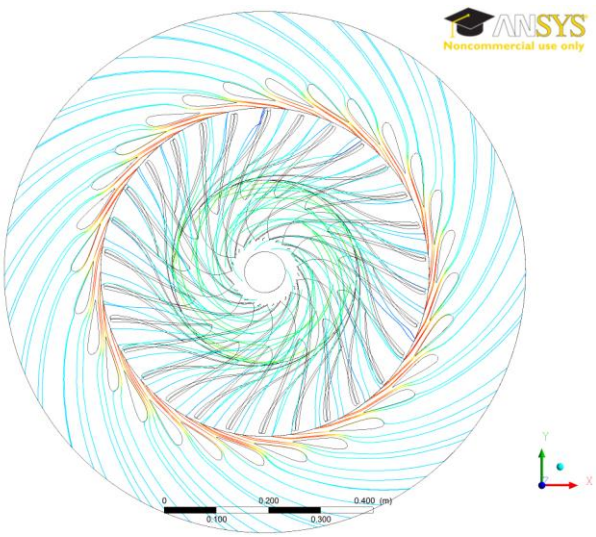

Figure 21: Rotating runner velocity streamlines

Y + values were studied at all surfaces within the runner. Figure 22 shows the Y + values at the runner blades and splitter blades. Most of the areas are within the range where the SST-turbulence model is applicable, except at the inlet, on the pressure side of the blades and splitter blades.

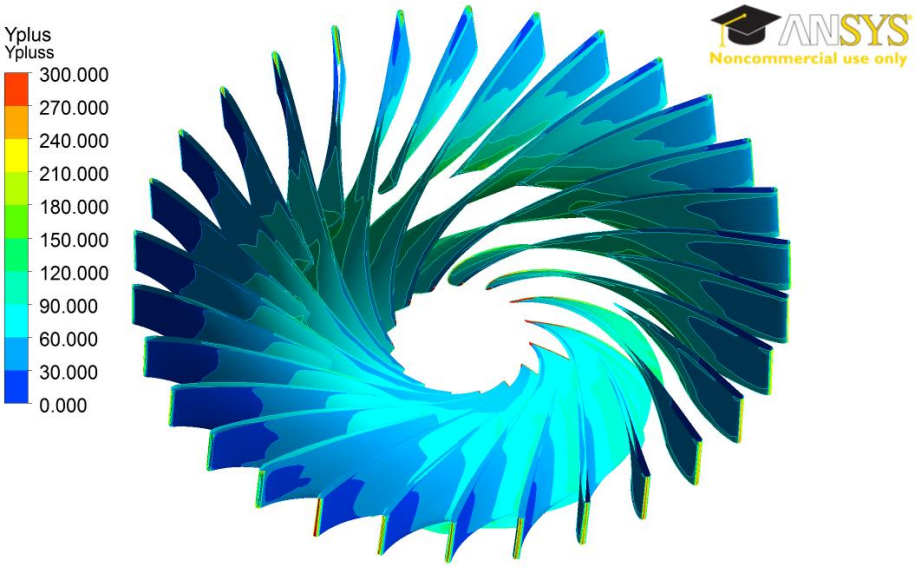

Figure 22: Y + at the blades and splitter blades

The Y + values of the shroud are shown in Figure 23. At the shroud smaller areas on the inlet pressure side, in proximity to the blades, the Y + are too low for the k- epsilon model, and too high for the k- omega model. Towards the outlet, the Y + values are too high, thus the turbulence model does not work.

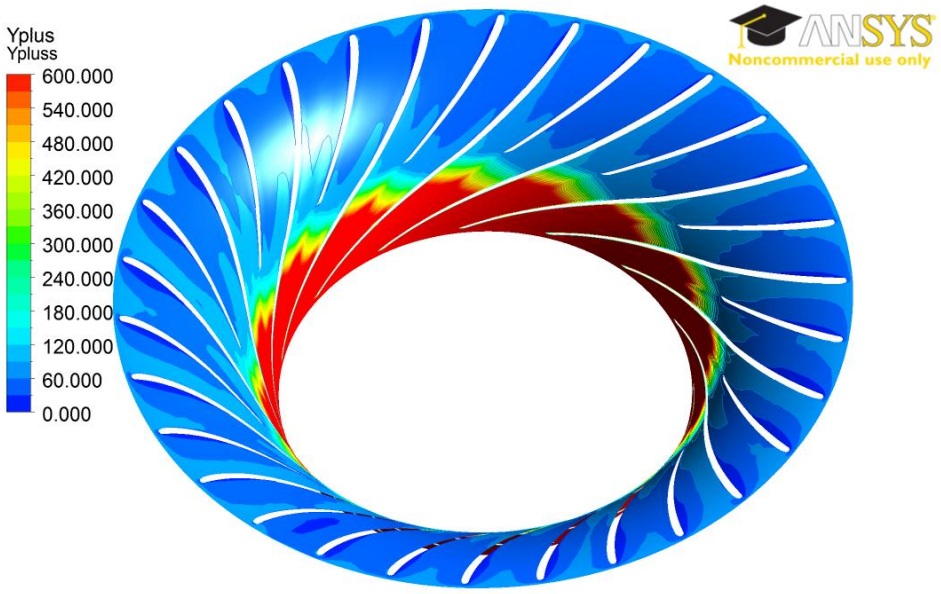

Figure 23: Y + at the shroud

The Y + values for the hub are shown in Figure 24. The Y + values are similar to the Y + values for the shroud. Smaller areas at the inlet and a bigger area towards the outlet have Y+ values which are inappropriate for the SST turbulence model.

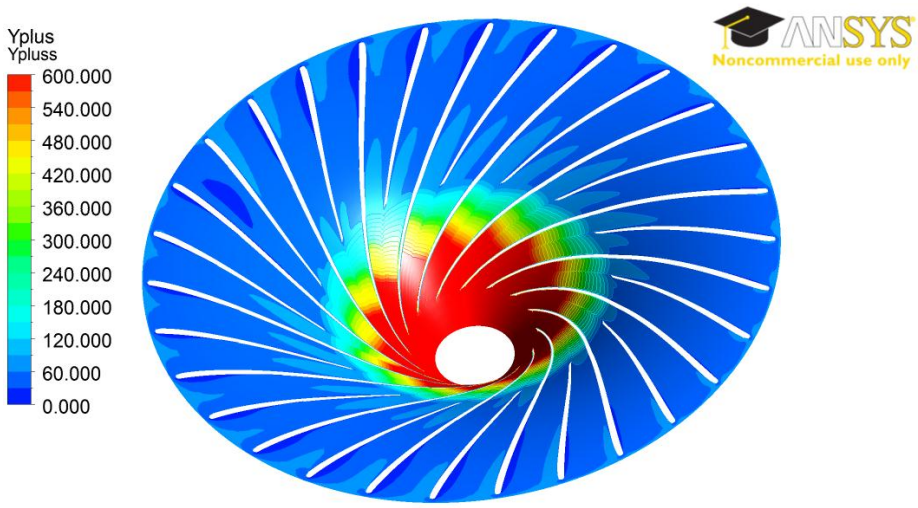

Figure 24: Y + at the hub

4.3 3D Model and mesh

In consultation with supervisor Ole Gunnar Dahlhaug, it was decided that the focus for the model only should be on the runner. The model is shown in Figure 25.

Figure 25: The Tokke turbine model

The mesh for the FEM analysis was created from this model. Before meshing, the model was slightly simplified.

Areas, from experience, which do not affect the results of the regions of interest, were smoothed out. This was done in order to simplify the meshing process, and avoid increasing mesh densities in areas which are not of specific interest. To reduce computational time, the FEM mesh only represents one part of the turbine. The final model for the FEM mesh is shown in Figure 26.

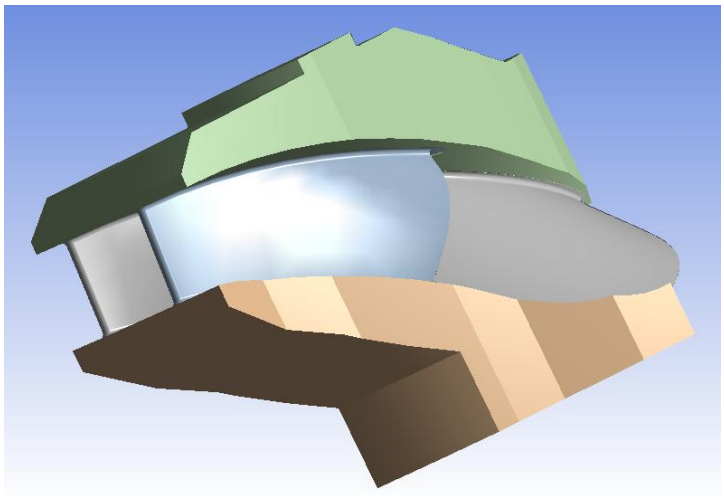

Figure 26: The FEM mesh model

The part consists of one blade and one splitter blade. The density of the mesh was defined by specifying the max elements size. Table 7, found in Appendix A, shows the main input data for the mesh with the highest density that could be created. A dense mesh is required in order to reduce areas of singularity.

The geometry for the CFD-mesh and the FEM- mesh were simplified in slightly different manners. This is due to the fact that the CFD- runner mesh was not originally created for FSI purposes. More than 90% of the nodes were mapped onto corresponding nodes at the FEM

mesh when the CFD results were applied. The remaining nodes were mapped onto the closet edge or node. Figure 27 shows the FEM mesh, and Figure 28 shows the quality.

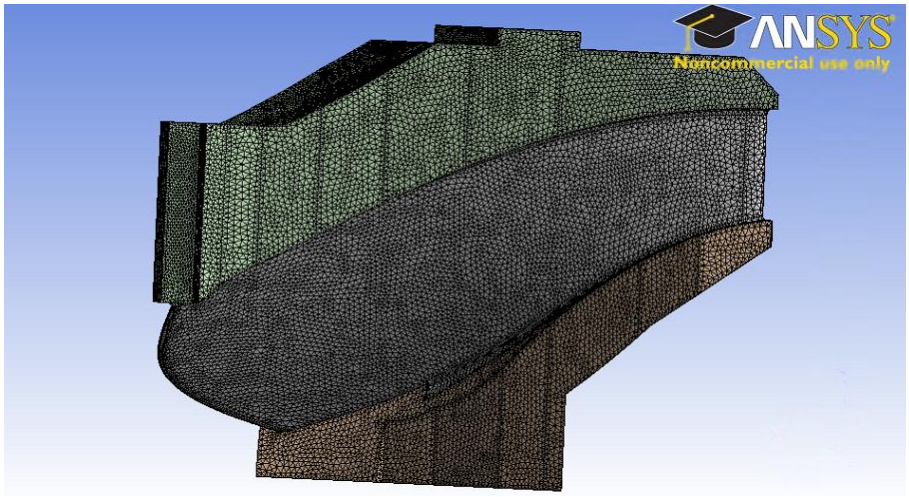

Figure 27: Element distribution in the FEM mesh

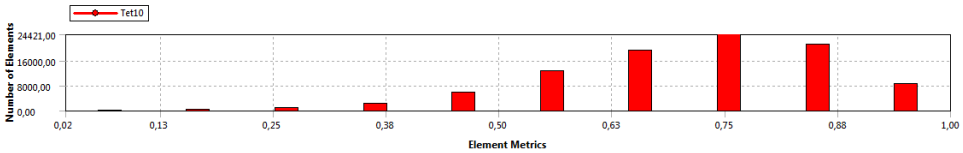

Figure 28: Quality of the FEM mesh

Figure 29 shows how the imported load solutions from the CFD results mapped onto the FEM model.

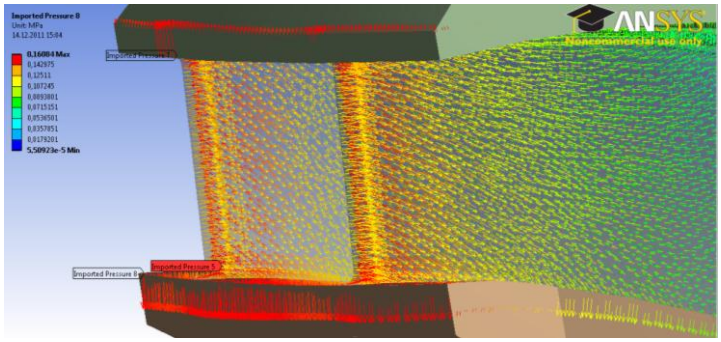

Figure 29: Imported load solution

Chapter 5: Results

5.1 CFD Results

To study pressure pulsations from the guide vanes, four steady state simulations were conducted. This was done by rotating the wicket gate mesh. There are 28 guide vanes in the wicket gate, hence the angle between two guide vanes are 360°/28≈12.857°. 4 sections within this angle were studied, thus the rotated angle between each mesh was set to; 12.86/4≈3.215°. Section 0 corresponds to a rotation of 0 degrees, section 1 to the 3.215, section 2 to 6.429 and section 3 to 9.463. Table 1 below shows the mean results of the simulations:

Net head	29.9	[m]
Runner hydraulic efficiency	94.19	[%]
Wicket Gate pressure loss	1.7	[m]

Table 1: CFD results

Figure 30 shows the pressure contours of a cross section of section 0, located horizontally in the middle of the inlet height. The pressure wake from the guide vanes propagate down the runner channels.

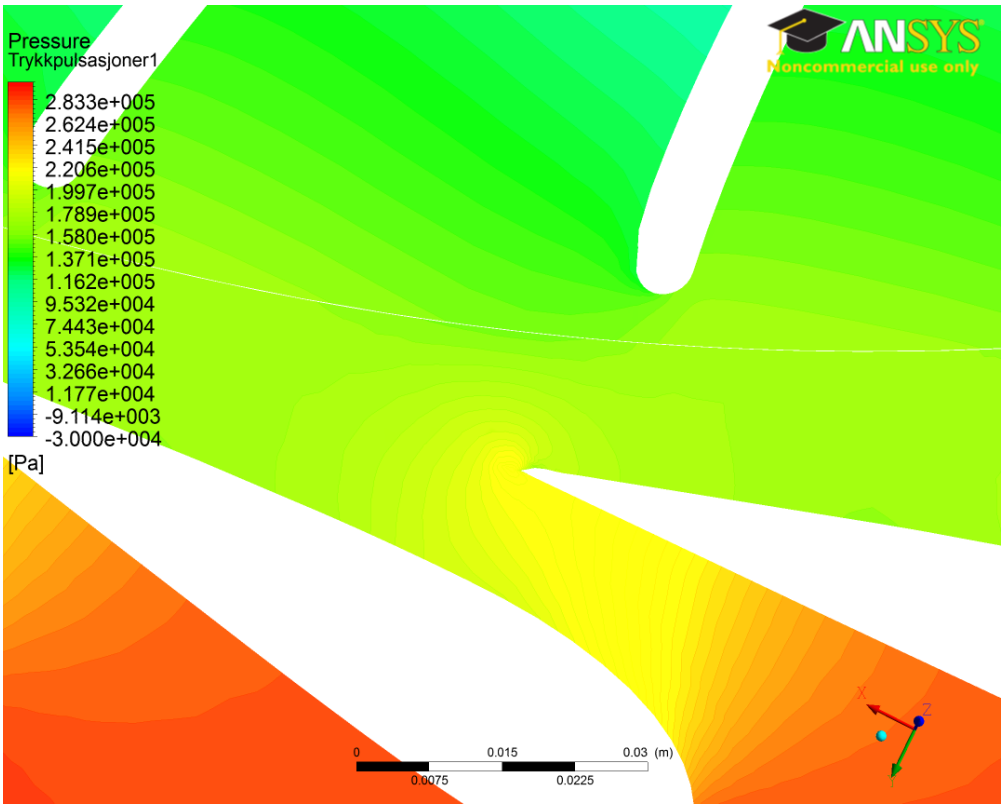

Figure 30: Pressure contour plot of one channel

In order to check the pressure pulsations from the guide vanes, the pressure in all the four sections were checked. This was done by specifying lines over which the pressure was investigated in one turbine channel. The positioning of the lines is shown in Figure 31. Number 1 is at the inlet, and the number increases towards the outlet.

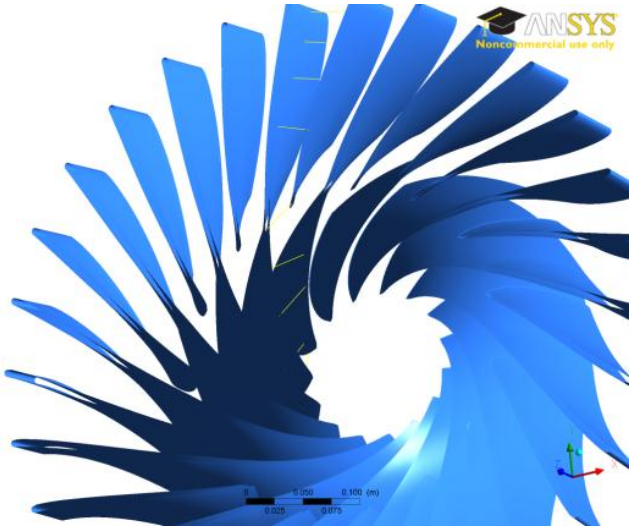

Figure 31: Line distribution

Figure 32- Figure 35 show the pressure over the lines at section 0- 3. The results show that there are smaller pressure differences over the lines for the different sections. The pressure difference induces a dynamic load at the runner structure.

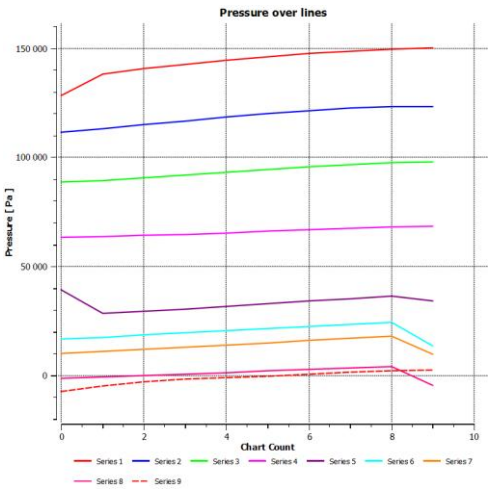

Figure 32: Pressure pulsations, section 0

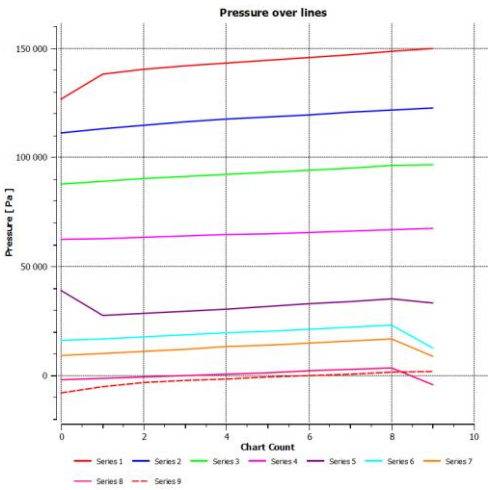

Figure 33: Pressure pulsations, section 1

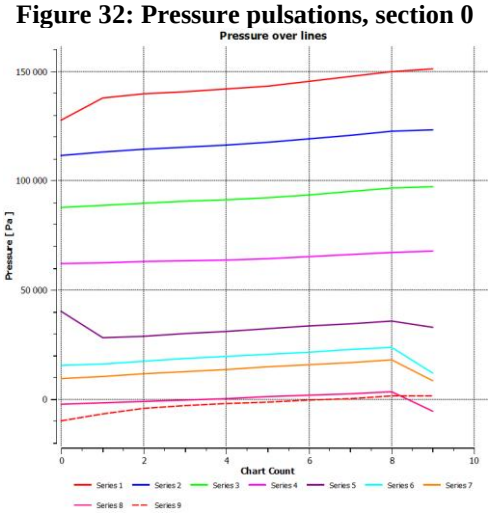

Figure 34: Pressure pulsations, section 2

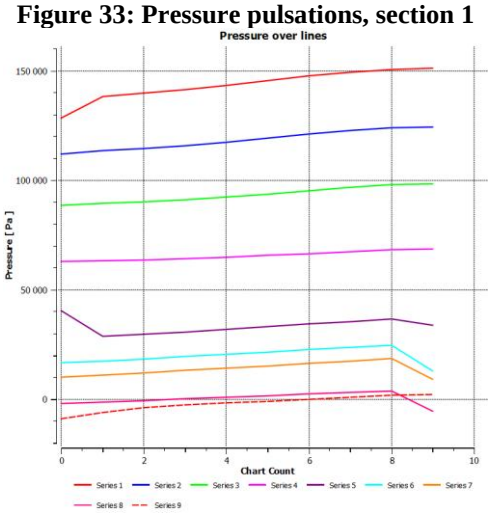

Figure 35: Pressure pulsations, section 3

5.2FSI Results

High stress zones were found at the trailing edge of the blade as shown in Figure 36. The four simulations show different results. Simulations with and without rotation of the runner were conducted. This was done because the results from Norconsult, presented in 5.3, did not apply rotation when determining the dynamic impact. High stress zones were studied at all four sections. Figure 36 shows the areas for investigation; the blades at the hub and shroud side at the outlet where higher stress zones were recorded.

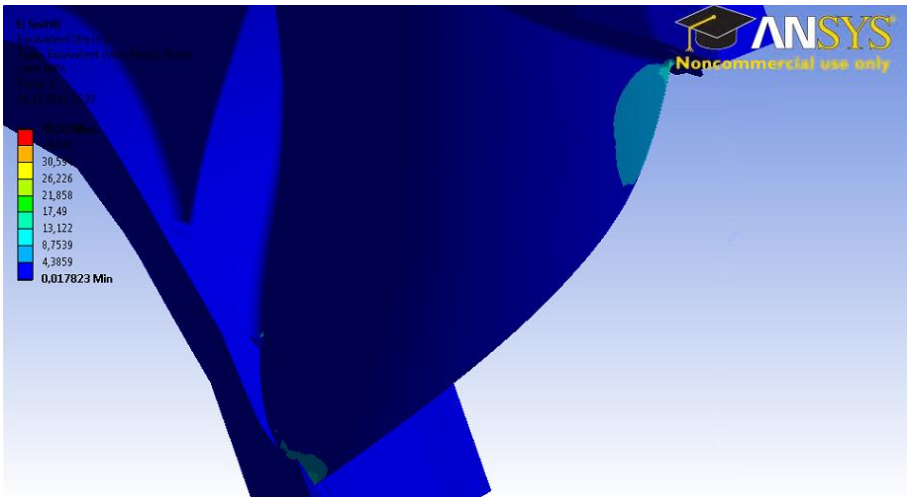

Figure 36: High stress zones

A probe was inserted in each high stress zone. Figure 37 shows the locations of the probes. Probe 1 is at the shroud side whereas probe 2 is at the hub side.

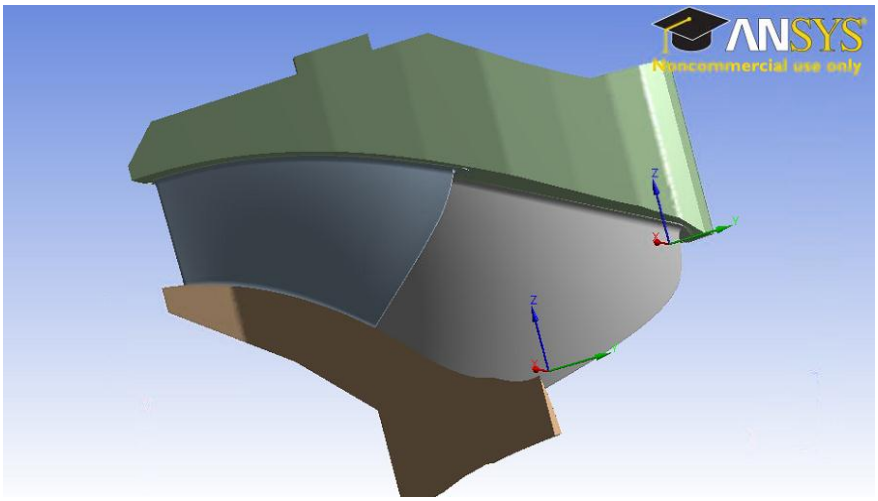

Figure 37: Probe Locations

Table 2 and Table 3 state the Von Mises stresses at both probe locations. In these tables the effect of the rotational velocity of the runner is omitted.

	Rotation [Degrees]	Von Mises Stress [Mpa]	Amplitude [Mpa]
Section 1	0	20,739	2,31975
Section 2	3,21429	16,058	-2,36125
Section 3	6,42857	15,51	-2,90925
Section 4	9,64285	21,37	2,95075
	Mean Stress	18,41925	
		Peak to Peak Amplitude	5,86

Table 2: Stresses at probe 1, without rotation

	Rotation [Degrees]	Von Mises Stress [Mpa]	Amplitude [Mpa]
Section 1	0	65,057	1,4495
Section 2	3,21429	65,382	1,7745
Section 3	6,42857	62,039	-1,5685
Section 4	9,64285	61,952	-1,6555
	Mean Stress	63,6075	
		Peak to Peak Amplitude	3,43

Table 3: Stresses at probe 2, without rotation

To include all the forces acting on the runner the rotational velocity also had to be taken into consideration. Figure 38 and Figure 39 show the stresses in a blade. The zones exposed to the highest stress were found at the hub and shroud side of the outlet, and along both the shroud and hub side connected to the blade. Another high stress zone is found at the shroud side on the leading edge of the blades.

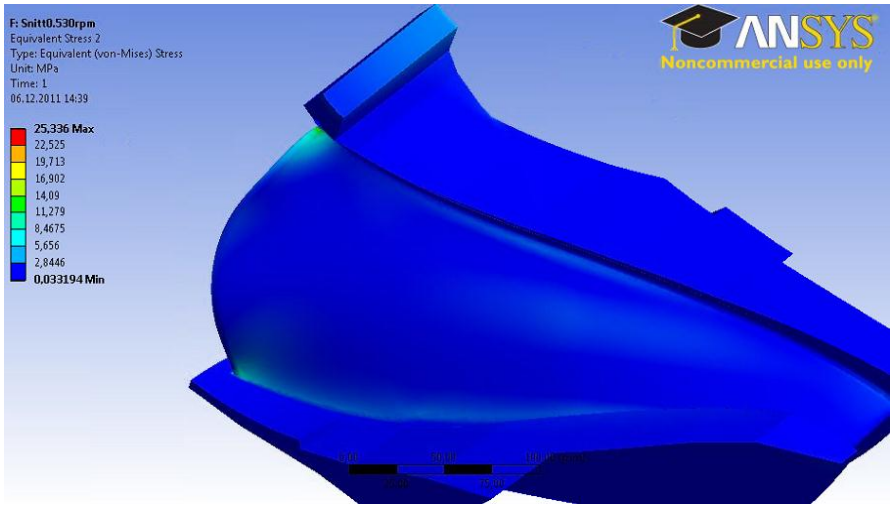

Figure 38: Von Mises Stresses at a runner blade, all forces included

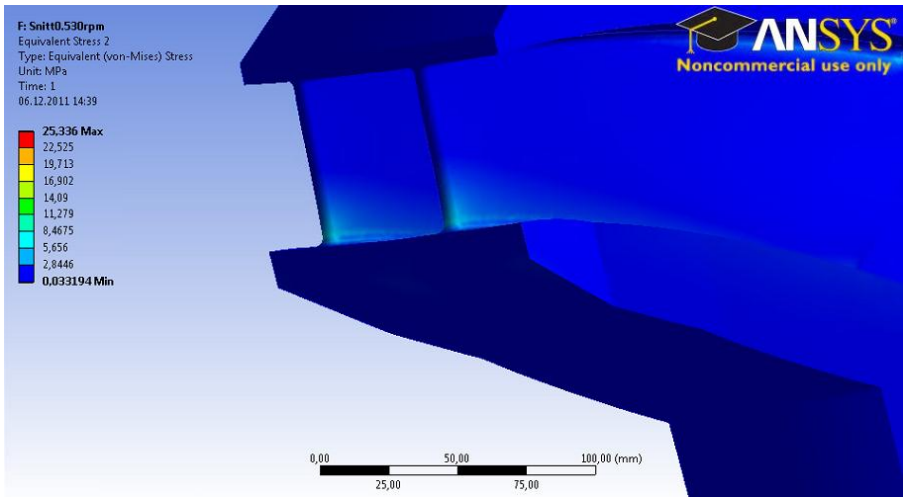

Figure 39: Von Mises Stresses at the inlet side, all forces included

5.3Laboratory results

Kobro (3) conducted pressure measurements of the Tokke Model Runner (3). His overall measurement results at BEP are the following:

Net head	30	[m]
Mechanical efficiency	93.5	[%]

Table 4: Laboratory results

Pressure measurements were also conducted at various places along the suction and pressure side at a runner blade. The results from the pressure measurements were applied to a FEM – model and is presented in "Mechanical robustness of Francis runners, requirements to reduce the risk of cracks in blades" by Bjørndal et al. (1). The mesh consists of a sector of the turbine containing both a blade and splitter blade. At the sides, periodic boundary conditions were used. The model was divided into sectors, in which the pressure data were inserted. In the regions between the measurement points linear interpolation was applied to state the pressure. A worst case scenario, were the dynamic load was applied over both the pressure and suctions side, was presented in the paper. The maximum calculated dynamic stress is 9.3Mpa, which is 67% of the mean static stress which is 13.8Mpa. The pressure is high at the inlet and drops towards the outlet. At the trailing edge, the blades become thinner and the stress levels increase. The trailing edge of a blade is sensitive to dynamic loading. Due to the fact that this paper focuses on the fatigue, rotational velocity was not applied to the FEM model as the additional stress impact would be uniform.

5.4 Lab results compared to FSI result

The results from the CFD calculations show the same trends as the results presented in the paper of Bjørndal et al. (1), increased stresses at the trailing edge in the transition between the

blade and the hub and the blade and shroud. The results from FSI analysis show larger higher static stresses and lover dynamic stresses.

The efficiency for the spiral casing is 99% (2), for the wicket gate 94.7% and for the runner 94.2%. This corresponds to an overall hydraulic efficiency of 88.3%. This is low in comparison to the mechanical efficiency of 93.5% measured by Kobro (3). The deviation in efficiency between FSI results and lab measurements is 5.2%. The efficiency losses for the CFD analysis includes; the spiral casing, guide vanes, leakage losses, which corresponds to domain interface connections, runner and draft tube. In addition to these losses, the efficiency measurements by Kobro (3) includes; turbine shaft and bearing losses.

Chapter 6: Discussion

The simulation results are close to the laboratory measurement results. As the results indicate in 5.4, is the deviation in efficiency between FSI results and lab measurements 5.2%. One reason for the deviation is the wicket gate grid. The pressure loss of the wicket gate used for the complete turbine analysis is 1.7m. This is too high, as the pressure loss for the finer mesh for the wicket gate is 0.65m. The wicket gate grid independency analysis is not completely converged, hence it is expected that the pressure loss would be smaller for denser meshes. Even though the pressure loss would decrease when using denser meshes, the pressure loss would still be high. One explanation for this is the exaggerated inlet length at the wicket gate. The wicket gate walls induce pressure drops. The wicket gate inlet length was exaggerated to obtain stable flow conditions upstream the guide vanes. If a denser mesh were used for the wicket gate, the overall simulated efficiency would approach the measured mechanic efficiency. This argument holds for the runner as well. The streamlines at the runner outlet shown in Figure 17 and Figure 18 are almost straight and without swirl. Hence the runner operates close to BEP. The CFD results in 5.1 show that the head of the turbine, wicket gate included, is approximately 29.9m. The model runner was tested for 30m. The pressure loss for the spiral casing is 0.3m (2). Hence, the net head at the simulations is approximately 30.2m. The deviation in net head between the lab measurements and the simulations is only 0.2m, which corresponds to a mismatch of less than 1%. The deviations in net head and efficiency between simulation results and laboratory measurement results are small and therefore considered to be satisfactory.

For the runner the convergence criterion was set to 10^{-5} and a first order solver was used. The residual for the draft tube, oscillates around 10^{-4}. In order to get lower residuals, a solver with higher order could be used. However, this was considered to be unnecessary, as the influence is minimal and the accuracy of the results is satisfactory for this work.

In order study the impact of from pressure pulsations from the guide vanes, two points in the runner blade were studied. The results in 5.2 show a stress peak to peak amplitude of 5.86Mpa, where the mean stress is 18.42Mpa. Hence the dynamic stress corresponds to 31.8% of the total stress. The other examination point shows a peak to peak amplitude of 3.43Mpa, where the mean stress is 63.31Mpa. The stress peak to peak amplitude corresponds to 5.4% of the mean stress. The stress differences are most likely due to pressure pulsations from the guide vanes, as dynamic stresses generally are totally dominated by pressure pulsations at normal operation range (1).

The calculated maximum dynamic stress for the model runner in (1) is 67% of the mean stress, 9.3Mpa of 13.8Mpa. The differences between the maximum stress of the laboratory measurements and simulations are probably due to the small differences in probe locations, but may also be a consequence of uncertainties in CFD and FEM simulations and measuring uncertainty. The result showing a mean stress of 63.31Mpa is high in comparison the maximum calculated stress in (1). The probe could have been inserted in an area of singularity. This would have explained the high mean stress. The dynamic load range for the

simulations could be greater if more simulations were conducted and thus a bigger load spectrum would be available. The turbine investigated is a model turbine. This means that the wetted surface is bigger than for the prototype and consequently the stresses are lower.

In case of fatigue, running at overload is the worst scenario within the normal operation range (1). The simulations were conducted close to BEP. Operation around BEP results in the minimal disturbance from the guide vanes (1). Hence, the pressure pulsations from the guide vanes at over load would increase the pressure pulsations. For low head runner operations around BEP do not cause fatigue (1). Hence, dynamic loading of the complete operation range should be further studied.

The CFD simulations were conducted for the complete turbine. To save computational time and to enhance the possibility to get denser meshes, it would be preferable to investigate one passage of the turbine. However, in order to detect all effects, the whole runner had to be simulated. This is because the runner is connected to a draft tube and the connection between the runner and turbine is two- way. This is also the case for the spiral casing. The water is not distributed evenly into the wicket gate (2). For the FEM mesh only one passage was modeled. This was done in order to save computational time and to create a denser mesh. As explained in 5.1 this is sufficient because one complete load cycle was investigated.

The geometry for the FEM-model is slightly modified in order to avoid problematic geometries which might not be meshed, e.g. the labyrinth bearing at the FEM model was smoothed out. This, however, does not influence the results, as the modified areas are far away from the areas of interest.

The mesh of the FEM model does not properly match the mesh of the CFD model. Approximately 90% of the nodes from the CFD mesh were mapped on matching nodes of the FEM model. The remaining nodes were mapped on to the closet edge or node. These small discrepancies do not significantly influence the results.

All meshes were created based on the techniques described in Appendix D. Mesh quality is detrimental do successful simulations. Computer capacity limited the number of elements that could be included in the runner and wicket gate grids. This reduced the possibility to obtain an adequate grid for the simulations. It would be preferable to have the opportunity to run grid independency analysis. The chance of obtaining correct results would have increased.

If new FSI analyses are to be performed, the designer can optimize the process by specifying what is really necessary for the simulations. The draft tube is not very important when doing FSI analysis of the runner. However, in order to get a converged solution, the outlet of the turbine should at least be prolonged as a cylinder. This should be done in order to avoid problematic outlet conditions. ANSYS Turbogrid supports creating one passage with periodic boundary conditions. In Design Modeler both the water path and the structure of the turbine can be specified. By doing so, an automatic FSI coupling is created. This will save modeling time and also give the possibility to perform two- way FSI analyses. The FSI analysis performed in the project is one- way.

In order to improve the integrity of the turbine several things can be done. Smaller changes in geometry may greatly influence the stress oscillations (1). The blade profile for the guide vanes can be optimized in order to create a smaller wake. The angle of attack could also be optimized in order to create as small wake as possible. The free space between the guide vanes and the runner could also be increased. The wake will get more time to mix out before entering the turbine without increasing the friction loss significantly. All the above mentioned examples could be done without decreasing the efficiency of the turbine. To compensate for the stress amplitude at the trailing edge the blade could be made thicker at the trailing edge. This would decrease the stress. However, increasing the thickness might negatively influence the efficiency of the turbine.

Chapter 7: Conclusion

FSI simulations of the Tokke turbine model were performed at conditions reported to be best efficiency point (BEP) and compared to lab measurements. The correlation is good, and would be even better if denser meshes could be applied. Computer power sat a limitation for the simulations, but this can be solved by running new simulations on more powerful computers.

The calculated maximum dynamic stress for the model runner in (1) is 67% of the mean stress, 9.3Mpa of 13.8Mpa. The differences between the maximum stress of the laboratory measurements and simulations are probably due to the small differences in probe locations, but may also be a consequence of uncertainties in CFD and FEM simulations and measuring uncertainty. The stress differences are due to pressure pulsations from the guide vanes. The dynamic load range for the simulations could also be greater if a bigger load spectrum would be available. In order to get the complete picture of the peak to peak amplitude, more simulations should be conducted.

The stress amplitude is expected to be higher at part- and overload. As operation around BEP results in the minimal disturbance from the guide vanes, the pressure pulsations from the guide vanes at part and over load would increase the pressure pulsations. Pressure pulsations at BEP do generally not cause fatigue. Both the FSI simulations and the lab measurements show that dynamic stress corresponds to a big percentage of the total stress. Determining the dynamic impact on the integrity of turbines by computer simulations has previously been impossible due to lack of computational power. This can now be done and should, as discussed in our paper, “Mechanical robustness of Francis runners, requirements to reduce the risk of cracks in blades” (1), be included as part of turbine design. In addition to the specifications currently provided, the energy companies should give operation plans in their specifications to the manufactures. The operations plans would give the turbine manufactures the necessary information so that dynamic loads can be accounted for.

Chapter 8: Further work

This project is a good basis for further analysis. In order to get a complete picture of the stress distribution in the Tokke turbine model, transient simulations should be conducted. If possible the simulations should be run on a powerful computer. This should be done in order to run simulations faster and to create denser meshes. The spiral casing for the Tokke turbine model could also be included. The mesh has already been made and could easily be coupled with the other meshes.

Simulations should also be conducted at other operation points than BEP. A program that automatically changes the guide vane opening angle has been created. Hence creating a setup for running simulations at part- and overload can be done quickly.

When a complete picture of the loading is obtained the stress variations could be compared to the Paris diagram and Wöhler curve in order to check for fatigue failures and cracks. After this is done, problematic areas can be detected, fixed and reinvestigated.

The guide vanes do not fully distribute the water evenly onto the runner. A wake is present. It would be interesting to quantify the impact the runner experiences due to wake. This can be done by running simulations for the wicket gate with and without guide vanes. Afterwards the wake effect can be quantified.

With CFD it is easier understand the physics of the flow. Areas of the flow which are hard to measure in lab are easy accessible in CFD. CFD shows the entire flow field. Hence, further work comprises getting a better understanding of the physics of the flow and how dynamic loading can be decreased without efficiency declination. Several of these things can be done without spending too much time, e.g. widen the wane less space for the wake to mix out before entering the turbine.

References, index of literature

1. *Mechanical robustness of Francis runners, requirements to reduce the risk of cracks in blades.* **Halvard Bjørndal, André P. Reynaud and Anders L. Holo.** Prague : Norconsult, 2011.

2. **Holo, Anders.** *CFD Anlysis of Distributor Flow.* s.l. : NTNU, 2011.

3. **Kobro, Einar.** *Measurement of Pressure pulsations in Francis Turbines.* Electronic ISBN: 978-82-471-2240-2 : NTNU, Doctoral theses at NTNU, 2010:136.

4. *Dynamic Stresses in a Francis Runner Based n Fluid Strucutre Interacion Analysis.* **Ruofo Xiao, Zhenqwei Wang and Yongyao Luo.** Beijing : Tsinghua Science & Technology, 2006.

5. **Breivik, Simen Røst.** *CFD- analysis of a runner and draft tube in a Francis turbine.* s.l. : NTNU, 2011.

6. **Antonsen, Øyvind.** *Unstady flow in wicket gate and runner with focus on static an dynamic load on runner.* Electronic ISBN: 978-82-471-3408-5 : NTNU, Theses at NTNU, 2007:155.

7. *CFD prediction of unsteady wicket gate-runner interaction in Francis turbines: A new standard hydraulic design procedure.* **Bernd Nennemann, Thi C.Vu, Mohamad Farhat.** Villach : s.n., 2005. Referance: LMH-CONF-2006-006.

8. CFD-online. *Best Pracitce Guidelines for turbomachinery.* [Online] [Cited: 12 18, 2011.] http://www.cfd-online.com/Wiki/Best_practice_guidelines_for_turbomachinery_CFD#Near-wall_treatment.

9. **H K Versteeg, W Malalasekera.** *An introduction to Computational Fluid Dynamics, The Finite Volume Method, second edition.* ISBN: 978-0-13-127498-3 : Pearson Prentice hall, 2006.

10. **White, Frank M.** *VISCOUS FLUID FLOW, Third Edition.* s.l. : McGRAW - HILL, 2006. ISBN: 007-124493-X.

11. **Brekke, Hermod.** *Grunnkurs i hydrauliske Strømningsmaskiner.* s.l. : Vannkraftlaboratoriet NTNU, 2000.

12. **Ansys, Inc.** *ANSYS 13.0 Help.* s.l. : Ansys Inc., 2010.

13. **RMB Consulting & Research, Inc.** RMB Consulting & Research, Inc. [Online] [Cited: 5 28, 2011.] http://rmb-consulting.com/newpaper/wall/lawgraph.gif.

14. **Fernandino, Maria.** Applied Computational Fluid Dynamics (TEP23). 6. Turbulence Modelling. Trondheim : s.n., 2008.

15. **Touzot, Gouri Dhatt and Gilbert.** *The Final Element Method Displayed.* 1982. 0471901105.

16. **Nilsen, Torbjørn K.** elkraft.ntnu.no. [Online] 10 14, 2005. [Cited: 12 2011, 18.] http://www.elkraft.ntnu.no/eno/bolgekraft/Turbinerforlavefall051014.pdf.

Appendix A Tables and figures

Important Domain Conditions		
Domain motion	Stationary	
Reference pressure	0	[Pa]
Wall friction	No slip walls	
Turbulence Model	SST	
Fluid	Water	
Guide Vanes opening angle	10	[^{o}]
Inlet conditions		
Mass flow inlet	310	[Kg/s]
Flow Direction		
Axial Component	0	[-]
Radial component	0.474342	[-]
Theta component	0.880341	[-]
Outlet conditions		
Static pressure outlet	0	[Pa]
Solver conditions		
Advection Scheme	High Resolution	
Turbulence Numeric	First Order	
Timescale factor	1	
Convergence target	10^{-5}	
Convergence type	RMS	

Table 5: Wicket gate simulations input values

Important Domain Conditions		
Turbulence Model	SST	
Wall friction	No slip walls	
Case	Stationary	
Guide Vane Domain		
Domain motion	Stationary	
Reference pressure	0	[Pa]
Mass flow inlet	310	[Kg/s]
Guide Vanes opening angle	10	[^{o}]
Fluid	Water	
Flow Direction		
Axial Component	0	[-]
Radial component	0.474342	[-]
Theta component	0.880341	[-]
Runner Domain		
Rotational speed	530	[rpm]
Draft Tube Outlet conditions		
Static pressure outlet	0	[Pa]
Interfaces between domains		
Connection	GGI	
Frame Change Model	Frozen Rotor	
Solver conditions		
Advection Scheme	High Resolution	
Turbulence Numeric	First Order	
Physical Timescale	0.01	[s]
Convergence target	10^{-5}	
Convergence type	RMS	

Table 6: Full turbine simulation input values

Important Domain Conditions		
Mesh type	Tetrahedrons	
Max element size	1.6	[mm]
Axial support	Fixed support	
Case 1		
Rotational velocity	0	[rpm]
Case 2		
Rotational velocity	530	[rpm]

Table 7: FEM input data

			Y+ Guide Vanes			Y + Walls			Total Pressure		
Case	Elements [-]	Nodes [-]	Min [-]	Average [-]	Max [-]	Min [-]	Average [-]	Max [-]	Inlet [kPa]	Outlet [kPa]	Difference [Pa]
1	2867336	812191	2,8	130,0	366,4	8,7	138,3	366,4	82,5	73,4	9 098,0
2	2995895	856025	3,8	135,7	350,5	8,1	144,5	350,5	82,6	73,9	8 708,0
3	3222713	929530	2,8	144,8	301,5	5,9	153,7	301,5	82,5	74,2	8 306,0
4	3573481	1033741	2,5	152,9	303,6	16,2	160,6	302,1	82,6	74,6	7 999,0
5	4067588	1175609	3,4	164,8	315,2	12,3	167,2	300,9	82,6	74,9	7 642,0
6	4754557	1360083	2,1	174,5	319,2	12,9	171,2	301,8	82,6	75,2	7 397,0
7	5648181	1592806	1,8	184,3	322,7	9,7	176,0	301,3	82,6	75,4	7 218,0
8	8143445	2220817	2,5	201,0	323,9	5,3	184,7	300,1	82,6	75,8	6 783,0
9	6813766	1891781	2,8	193,9	323,9	11,4	180,8	301,3	82,5	75,6	6 973,0
10	6807550	1890781	2,1	193,8	324,0	10,8	181,0	300,7	82,5	75,5	7 002,0
11	6803929	1890260	2,6	194,0	324,0	9,9	181,0	300,9	82,5	75,5	6 990,0
12	8142683	2220396	3,1	201,1	323,9	5,2	184,7	300,1	82,6	75,8	6 790,0
13	9750351	2608453	3,1	209,1	324,5	10,3	185,9	305,9	82,7	76,1	6 625,0
14	12437069	2262986	1,6	252,1	626,4	5,5	263,0	536,7	85,1	78,6	6 505,0

Table 8: Wicket gate analysis results

Appendix B CFD and FEM

This chapter contains theory about CFD and FEM.

CFD Theory

CFD is widely used in the industry to solve fluid flow and heat exchange problems. CFD may quickly obtain accurate results for a low cost comparing to e.g. costly laboratory tests (9).

With CFD simulations for water power one normally solves two governing equations.

Navier Stokes equation (Newton's second law applied to continuous fluids (10):

$$\begin{aligned}
\frac{\partial \rho}{\partial t}(\rho u_x) + div(\rho u_x \vec{u}) &= -\frac{\partial p}{\partial x} + \frac{\partial \tau_{xx}}{\partial x} + \frac{\partial \tau_{yx}}{\partial y} + \frac{\partial \tau_{zx}}{\partial z} + \rho f_x \\
\frac{\partial \rho}{\partial t}(\rho u_y) + div(\rho u_y \vec{u}) &= -\frac{\partial p}{\partial y} + \frac{\partial \tau_{xy}}{\partial x} + \frac{\partial \tau_{yy}}{\partial y} + \frac{\partial \tau_{zy}}{\partial z} + \rho f_y \\
\frac{\partial \rho}{\partial t}(\rho u_z) + div(\rho u_z \vec{u}) &= -\frac{\partial p}{\partial z} + \frac{\partial \tau_{xz}}{\partial x} + \frac{\partial \tau_{yz}}{\partial y} + \frac{\partial \tau_{zz}}{\partial z} + \rho f_y
\end{aligned} \qquad [2]$$

$\vec{f}$ represents the body forces which for turbo machinery consist of the centrifugal force and the Coriolis force. The formula is listed below (11).

$$\vec{f} = \vec{\omega} \times \left(\vec{\omega} \times r\right) - 2\left(\vec{\omega} \times \vec{u}\right) \qquad [3]$$

Also the conservation of mass equation has to be solved. White (10) gives the conservation of mass formula:

$$\frac{\partial \rho}{\partial t} + div(\rho \vec{u}) = 0 \qquad [4]$$

All these equations are written in conservative form which relate to infinite small elements in a fluid flow. In CFD calculations a volume is dived into numerous small cells in which all the governing equations of CFD calculation are solved. At each point where the cells are connected there is a node, except for a staggered grid which has a more complex nodal distribution. Within the nodes the calculations take place, hence the node contain the information regarding the solutions of the governing equations. To solve the equations at the node, a node gathers information from its neighboring nodes and neighbors neighbor nodes.

This may be done in several ways depending on which numerical scheme is chosen for the particular case.

Different types of numerical schemes have strengths and weaknesses regarding accuracy, computational cost, and time. Numerical schemes are found within the solvers in a CFD program. Appropriate schemes for various cases may be found in scientific reports. A solver uses a numerical scheme by default. Numerical schemes are not further discussed in this text. More information regarding solvers is found in (12).

CFD Grid

Preprocessing is an important and laborious part of CFD calculations. In order to get reliable results from CFD the mesh plays a vital role. The model gets divided into nodes, surfaces and volumes which later can be solved numerically. Accurate simulations may be conducted without using turbulence models. However, this requires a huge amount of data storage capacity due to necessity of finer meshes as the number of nodes needed is approximately $Re^{9/4}$ (9).

Turbulence Modeling

Boundary layers are present in fluid flows and can be divided into three separate zones.

1. Viscous sub layer: Viscous shear is the dominant factor
2. Buffer layer: Velocity and turbulence are dominating factors.
3. Overlap layer: Both viscous and turbulent shears are important

A graphical representation of the logarithmic overlap layer is shown in Figure 40.

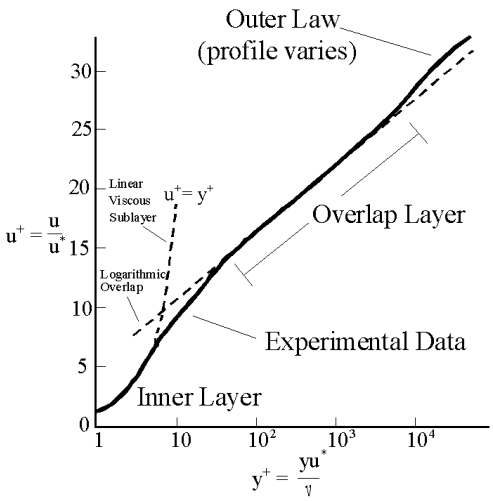

Figure 40: Logarithmic overlap law (13)

There are several turbulence models available each having its strengths and weaknesses. In this master thesis the shear stress transport (SST) turbulence model has been applied.

The SST turbulence model combines to widely used turbulence models, k-omega and k-epsilon. The k- omega is used from the wall to the viscous- sub layer and the k- epsilon is used for the free stream.

The k- epsilon model makes use of a universal behavior of near wall flow at high Reynolds numbers. The mean velocity satisfies the log law which indicate that in the region of 30<Y+<500 (9) the shear stress varies slowly with the distance from the wall. This takes place in the overlap layer. Y+ is a dimensionless distance from the wall to first node. Best practice indicate that Y+ values should be somewhere between 20<Y+<200 (8). Due to the slow variation the shear stress is modulated to be equal to the wall shear stress. The k-omega turbulence is valid in the range 0<Y+<2 (12). The Y+ formula is stated below (9).

$$y^+ = \frac{yu^*}{\nu} \qquad [5]$$

$$u^* = \sqrt{\frac{\tau_w}{\rho}} \qquad [6]$$

$$\tau_w = \mu\left(\frac{\partial u}{\partial y}\right)_{y=0} \qquad [7]$$

For the log law:

$$u^+ = \frac{1}{\kappa}\ln(y^+) + B = \frac{1}{\kappa}\ln(Ey^+) \qquad [8]$$

The SST model uses the following equations:

The Wilcox model:

$$\frac{\partial(pk)}{\partial t}+\frac{\partial}{\partial x_j}(\rho U_j k)=\frac{\partial}{\partial x_j}\left[(\mu+\frac{\mu_t}{\sigma_{k1}})\frac{\partial k}{\partial x_j}\right]+P_k-\beta'\rho k\omega \qquad [9]$$

$$\frac{\partial(\rho\omega)}{\partial t}+\frac{\partial}{\partial x_j}(\rho U_j \omega)=\frac{\partial}{\partial x_j}\left[(\mu+\frac{\mu_t}{\sigma_{\omega 1}})\frac{\partial \omega}{\partial x_j}\right]+a_1\frac{\omega}{k}P_k-\beta_1\rho\omega^2 \qquad [10]$$

And the transformed k – epsilon model:

$$\frac{\partial(pk)}{\partial t}+\frac{\partial}{\partial x_j}(\rho U_j k)=\frac{\partial}{\partial x_j}\left[(\mu+\frac{\mu_t}{\sigma_{k2}})\frac{\partial k}{\partial x_j}\right]+P_k-\beta'\rho k\omega \qquad [11]$$

$$\frac{\partial(\rho\omega)}{\partial t}+\frac{\partial}{\partial x_j}(\rho U_j \omega)=\frac{\partial}{\partial x_j}\left[(\mu+\frac{\mu_t}{\sigma_{\omega 2}})\frac{\partial \omega}{\partial x_j}\right]+2\rho\frac{1}{\sigma_{\omega 2}\omega}\frac{\partial k}{\partial x_j}\frac{\partial \omega}{\partial x_j}+a_2\frac{\omega}{k}P_k-\beta_2\rho\omega^2 \qquad [12]$$

Where:

$$\beta'=0.09$$

$$\alpha_1=5/9$$

$$\beta_1=0.075$$

$$\sigma_{k1}=2$$

$$\sigma_{\omega 1}=2$$

$$\alpha_2=0.44$$

$$\beta_2=0.0828$$

$$\sigma_{k2}=1$$

$$\sigma_{\omega 2}=1/0.856$$

The Wilcox model equations are multiplied by a function F_1, the transformed- epsilon equations is multiplied by a function 1- F_1. The BSL model reads (12):

$$\frac{\partial(\rho\kappa)}{\partial t}+\frac{\partial}{\partial x_j}(\rho U_j k)=\frac{\partial}{\partial x_j}\left[(\mu+\frac{\mu_t}{\sigma_{k3}})\frac{\partial k}{\partial x_j}\right]+P_k-\beta'\rho k\omega+P_{kb} \qquad [13]$$

And:

$$\frac{\partial(\rho\omega)}{\partial t}+\frac{\partial}{\partial x_j}(\rho U_j\omega)=$$
$$\frac{\partial}{\partial x_j}\left[(\mu+\frac{\mu_t}{\sigma_{\omega 3}})\frac{\partial\omega}{\partial x_j}\right]+P_k(1-F_1)2\rho\frac{1}{\sigma_{\omega 2}\omega}\frac{\partial k}{\partial x_j}\frac{\partial\omega}{\partial x_j}-a_3\frac{\omega}{k}P_k-\beta_3'\rho k\omega^2+P_{\omega b} \qquad [14]$$

The a coefficient in P_{wb} is replaced by a new coefficient, a3. A linear combination is formed from the coefficient underlying models to form the new coefficient.

$$\Phi_3=F_1\Phi_1+(1-F_1)\Phi_2$$

Blending functions are used to make the method successful. More about blending function is found in (12). To avoid extensive buildup of turbulent kinetic energy in stagnation regions, limiters for the production terms are used. More about limiters is found in (12).

Different turbulence models have both strengths and weaknesses. A widely validated turbulence model is the k-epsilon model. It has succeeded in calculating various recirculating and thin shear layer flows without adjusting the model constants case-by-case. The model applies the Y+ method, which uses a logarithmic overlap law to describe the boundary layer nearby a wall. Versteeg and Malalasekera (9) lists advantages and disadvantages for the k – epsilon model:

Advantages:

- Simplest turbulence model for which only initial and/or boundary conditions need to be supplied
- Excellent performance for many industrial relevant flows
- Well established, the most widely validated turbulence model

Disadvantages:

- More expensive to implement than mixing length model
- Poor performance flows with large extra strains (e.g. curved boundary layers, swirling flows)

Fernandino (14) lists the following advantages and disadvantages for the k- omega models:

Advantages:

- Better behavior than k – epsilon in separation regions
- Better behavior close to solid walls
- Easier boundary conditions at solid walls than k- epsilon

Disadvantages:

- Expensive, new empirical constants
- Same drawbacks as k- epsilon

Frame change modeling

The Frozen Rotor model treats the flow by maintaining the relative position of the components while changing the frame of reference. This model is preferable for non-axissymmetric flow domains such as e.g. turbine/draft tube and impeller/volute. The frozen rotor model is robust and uses less computer resources than the other frame changing models. A drawback for the model, among others, is in inadequate prediction of physics for local flow values (12).

Connection between domains

A GGI connection permits non-matching grids to be merged. All model options within CFX support GGI connections. The GGI connections permit models where there is a small gap between the meshes to be linked. When referring to small, this means where the gap is less than ½ the size of the average depth of the elements peripheral elements of each domain (12).

FEM Linear Static structural Analysis

FEM is a technique to obtain numerical solutions. This is used for cases where the analytical solutions are laborious or even impossible to find. FEM is widely used in industry today. The theory presented below is extracted from Touzot et al. (15).

A static structural analysis calculates displacements, body forces, strain and stress for cases that ate not heavily affected by inertia and damping effects. A static structural analysis contains algorithms for solving both linear and nonlinear deformations.

The Galerkin integral converts the continuous operator into a discrete problem:

$$W = \int_V \delta u \left(\xi(u) + f_V \right) dV \qquad [15]$$

The integral is discretized and replace by a summation:

$$W = \sum_{e=1}^{n_{e1}} \int_{V^e} \delta u^e \left(\xi(u) + f_V \right) dV = 0 \qquad [16]$$

Now each term W^e, u and δu are replaced by an finite element approximation:

$$\begin{aligned} u^e &= \langle N \rangle \{u_n\} \\ \delta u^e &= \langle N \rangle \{\delta u_n\} \end{aligned} \qquad [17]$$

$\langle N \rangle$ is zero outside the region of V^e and is only dependent of the nodal value $\langle u_n \rangle$ belonging to V^e. The computational process is confined to the element domain and it is the repetitive nature of the elementary matrices computation that contributed to the success of the method (15).

$$\begin{aligned} W^e &= \int_{V^e} \delta u^e \left(\xi(u^e) + f_V \right) dV \\ W^e &= \langle \delta u^e \rangle \left(\int_{V^e} \{N\} \xi(\langle N \rangle) dV \{u_n\} + \int_{V^e} \{N\} f_V dV \right) \end{aligned} \qquad [18]$$

Written in matrix notation we get:

$$W^e = \int_{V^e} \left(\langle \delta(\partial u^e) \rangle [D] \{\partial u^e\} - \partial u^e . f_v \right) dV - \int_{S_f^e} du^e . fsdS \qquad [19]$$

Where:

$$\langle \partial u^e \rangle = \left\langle u^e \frac{\partial u^e}{\partial x} \ldots \frac{\partial^2 u^e}{\partial x^2} \ldots \right\rangle$$

$$\langle \delta(\partial u^e) \rangle = \left\langle \delta u^e \delta \begin{pmatrix} \partial u^e \\ \partial x \end{pmatrix} \ldots \delta \begin{pmatrix} \partial^2 u^e \\ \partial x^2 \end{pmatrix} \ldots \right\rangle$$

By using [17] and putting it into [19] we get the discretized element integral with the following matrix form:

$$W^e = \langle \delta u_n \rangle \left([k] \{u_n\} - \{f\} \right) \qquad [20]$$

The symbols used are listed below:

f_v and f_s are body surface tractions.

V_e is the volume element

$[D]$ is matrix independent of u^e and its derivatives for linear derivatives.

s_f^e is the part of the boundary of part of v^e at which additional contour integral forms appear when integration by parts is performed.

$[k]$ is the element matrix

$\{f\}$ is the element load vector

$\{u_n\}$ is the element vector of nodal values

$\{\delta u_n\}$ is the first variation of the element nodal values

The summation of the element integrals forms the integral:

$$W = \sum_e W^e = \sum_e \langle \delta u_n \rangle \left([k]\{u_n\} - \{f\} \right) = 0 \qquad [21]$$

By a merging process we get the overall global matrix:

$$W = \langle \delta U_n \rangle \left([K]\{U_n\} - \{F\} \right) = 0 \qquad [22]$$

Where:

$[K]$ is the global system matrix

$\{F\}$ is the global right hand side load vector

$\{U_n\}$ is the global vector of all nodal values

$\{\delta U_n\}$ is an arbitrary variation of U_n

Since $W = 0$ for all values of $\langle \delta U_n \rangle$ it follows that:

$$[K]\{U_n\} = \{F\} \qquad [23]$$

The element residual function is as follows:

$$\{r\} = \{f\} - [k]\{u_n\} \qquad [24]$$

And consequently the global residual is:

$$\{R\} = \sum_e \{r\} = \{F\} - [K]\{U_n\} \qquad [25]$$

The residual diminish when $\{u_n\}$ approaches the exact solution.

To calculate the stress the Von Mises stress equation is applied.

$$\sigma_e = \left[\frac{(\sigma_1 - \sigma_2)^2 + (\sigma_2 - \sigma_3)^2 + (\sigma_3 - \sigma_1)^2}{2} \right]^{1/2} \qquad [26]$$

Where σ_e is the von Mises stress in an element, which let the principal stress values be represented by one single value.

Elements of uncertainty

In CFD calculations uncertainties and errors are important conditions that have to be considered when evaluating results (9). Miscalculations like round off errors, discretization errors, convergence, modeling errors occur. E.g. turbulence models reduce the resolution requirements in many orders of magnitude. The model calibrates the coefficients against experimental data for certain classes of flows (12).

Uncertainty is also linked to input values, geometry, material properties and boundary conditions. It is important to quantify the impact of uncertainty. This can be done by e.g. comparing results to laboratory measurements.

In FEM modeling singularity values are likely to erect. Areas of singularity are places where elasticity equations give infinite stress. This can happen in e.g. places where a load is directly applied. It is important to localize such values when e.g. maximum stress values are to be considered.

Appendix C Francis turbine

A Francis turbine consists of 4 main parts.

1. Spiral casing which distributes the water evenly onto the circumference of the guide vane operating mechanism.
2. Guide vane operating mechanism which obtains a uniform flow pattern, makes the water spin around the turbines z-axis towards the runner and regulates the water flow. The guide vanes may be remote-controlled by use of servomotors. The turbine influences the flow conditions in the distributor e.g. pressure pulsations arise when a runner blade passes a guide vane (14).
3. Runner which transforms the specific energy to mechanical energy. The runner consists of hub, shroud and blades. The runner is the only rotating part in the system.
4. Draft tube which reduces the danger of cavitation. The draft tube has a conic shape in which the velocity decelerates in order to regain the pressure.

The succeeding chapter gives the theory for the wicket gate and runner. The theory has been extracted from Brekke (11). The symbol list is found in Nomenclature:

Guide vanes and Runner

To understand how the turbine works the velocity of the water is decomposed into velocity components;

- Relative velocity direction along the blades, w – direction
- Tangential velocity component, u - direction,
- Absolute velocity direction, c- direction.

Figure 41 shows the velocity components.

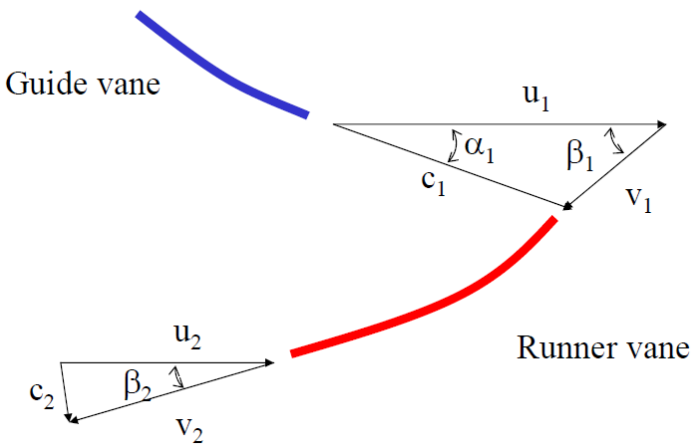

Figure 41: Velocity triangles (16)

The volume flow is defined by:

$$Q = c_{m1} 2\pi r_1 B_1 \qquad [27]$$

The main purpose of the guide vane is to regulate the water flow by adjusting the opening angle α. Downstream the guide vanes the water flows into a vane less space. The rotation through the vane less space is constant, as no forces are present to influence the rotation. Hence;

$$\vec{r} \times \vec{c} = \vec{r}_0 \times \vec{c}_0 = \vec{r}_1 \times \vec{c}_1 \qquad [28]$$

The force acting on a volume element dv which is influenced by the absolute acceleration (Newton second law) is given by;

$$\vec{F} = m\vec{a} = \iiint_V \frac{D\vec{c}}{Dt} \rho dV \qquad [29]$$

Hence;

$$\vec{M} = \iiint_V \frac{D}{Dt}(\vec{r} \times \vec{c}) dV \qquad [30]$$

By differentiating the expression we get:

$$\frac{D}{Dt}(\vec{r} \times \vec{c}) = \frac{\partial(\vec{r} \times \vec{c})}{\partial t} + (\vec{c} \cdot \nabla)(\vec{r} \times \vec{c}) \qquad [31]$$

For stationary flow the following term is cancelled:

$$\frac{\partial(\vec{r} \times \vec{c})}{\partial t} = 0 \qquad [32]$$

The last component in [31] can be written as:

$$(\vec{c} \cdot \nabla)(\vec{r} \times \vec{c}) = c_r \frac{\partial(\vec{r} \times \vec{c})}{\partial r} + c_u \frac{\partial(\vec{r} \times \vec{c})}{\partial u} + c_z \frac{\partial(\vec{r} \times \vec{c})}{\partial z} \qquad [33]$$

Now, we can include the c_r , c_u , and c_z in the parenthesis by using the following rule of differentiation:

$$\begin{aligned}
\frac{\partial(c_r\vec{R})}{\partial r} &= c_r\frac{\partial\vec{R}}{\partial r} + \vec{R}\frac{\partial c_r}{\partial r} \\
\frac{\partial(c_u\vec{R})}{\partial u} &= c_u\frac{\partial\vec{R}}{\partial u} + \vec{R}\frac{\partial c_u}{\partial u} \\
\frac{\partial(c_z\vec{R})}{\partial z} &= c_z\frac{\partial\vec{R}}{\partial z} + \vec{R}\frac{\partial c_z}{\partial z}
\end{aligned} \qquad [34]$$

Where:

$$\vec{R} = \vec{r}\times\vec{c} = \vec{e}_r R_r + \vec{e}_u R_u + \vec{e}_z R_z \qquad [35]$$

From these equations we now have:

$$(\vec{c}\cdot\nabla)(\vec{r}\times\vec{c}) = \frac{\partial(c_r\vec{R})}{\partial r} + \frac{\partial(c_u\vec{R})}{\partial u} + \frac{\partial(c_z\vec{R})}{\partial z} - \vec{R}(\nabla\cdot c) \qquad [36]$$

From incompressible flow we know that $c\cdot\nabla = 0$

By dividing the equation into factors, which is convenient due to the geometry where $\vec{R}_u$ is the vector about the u-axis, $\vec{R}_r$ is the vector about the r-axis and $\vec{R}_z$ is the vector about the z axis, we get;

$$\begin{aligned}
(\vec{c}\cdot\nabla)(\vec{r}\times\vec{c}) &= \vec{e}_r\frac{\partial(c_r R_r)}{\partial r} + \frac{\partial(c_u R_r)}{\partial u} + \frac{\partial(c_z R_r)}{\partial z} + \\
\vec{e}_u\frac{\partial(c_r R_u)}{\partial r} &+ \frac{\partial(c_u R_u)}{\partial u} + \frac{\partial(c_z R_u)}{\partial z} + \vec{e}_z\frac{\partial(c_r R_z)}{\partial r} + \frac{\partial(c_u R_z)}{\partial u} + \frac{\partial(c_z R_z)}{\partial z}
\end{aligned} \qquad [37]$$

Now we can replace the $(\vec{c}\cdot\nabla)(\vec{r}\times\vec{c})$ part in the moment equation, and we get:

$$\vec{M} = \iiint_V \frac{D}{Dt}(\vec{r}\times\vec{c})dV = \iiint_V [\vec{e}_r\nabla\cdot(R_r\vec{c}) + \vec{e}_u\nabla\cdot(R_u\vec{c}) + \vec{e}_z\nabla\cdot(R_z\vec{c})]\rho dV \qquad [38]$$

By using the Gauss theorem where ($\vec{n}$ is the normal vector on an arbitrary surface),

$$\iiint_V [\nabla\cdot\vec{u}dV = \iint_A \vec{u}\cdot\vec{n}dA \qquad [39]$$

We get:

$$\vec{M} = \iiint_V [\vec{e}_r \nabla \cdot (R_r \vec{c}) + \vec{e}_u \nabla \cdot (R_u \vec{c}) + \vec{e}_z \nabla \cdot (R_z \vec{c})] \rho dV = \iint_A [\vec{e}_r R_r + \vec{e}_u R_u + \vec{e}_z R_z] \rho (\vec{c} \cdot \vec{n}) dA \quad [40]$$

Where $(\vec{c} \cdot \vec{n}) dA = dQ$ which is the volume flow. Hence we get:

$$\vec{M} = \iint_A (\vec{r} \times \vec{c}) \rho dQ \quad [41]$$

And:

$$\vec{M}_z = \iint_A r c_u \rho dQ = \sum (r c_u)_{in} \rho Q_{out} - \sum (r c_u)_{out} \rho Q_{in} \quad [42]$$

Continuity gives $\dot{m}_{in} = \dot{m}_{out} = \rho c_{m1} 2\pi r_1 B = \rho c_{m2} 2\pi r_2^2 = \rho Q$

Consequently:

$$\vec{M}_z = \rho Q (c_{u1} r_1 - c_{u2} r_2) \quad [43]$$

And therefore the power becomes;

$$P = M_z \omega = \rho Q (c_{u1} r_1 - c_{u2} r_2) \omega = \rho Q E_t \quad [44]$$

Where E_t is the specific energy delivered by the water to the runner.

$$E_t = \omega (c_{u1} r_1 - c_{u2} r_2) \quad [45]$$

Where: $u = \omega r$

And thus:

$$E_t = c_{u1} u_1 - c_{u2} u_2 \quad [46]$$

The hydraulic efficiency is given by:

$$\eta_h = \frac{Extracted\,Energy}{Available\,Energy} \quad [47]$$

And:

$$\eta_h = \frac{1}{gH} (c_{u1} u_1 - c_{u2} u_2) \quad [48]$$

Appendix D Working process

This chapter presents the way to perform CFD and FEM calculations and the way this project work was done. The guidelines are based on the experiences form this project.

1. **Attend Classroom training or examine tutorials**
   Prior to conducting meshes and simulations the user should get an overview of numbers of tools which are at his disposal. This can be done by either examine tutorials or attend formal classroom training. There are always tips and tricks which can be suitable for your case which you will learn that you would never pick up on your own. Investing time in this process may save you for a lot of time afterwards.

2. **Make a model of the material/fluid**
   When the model is finished it should be visually checked for errors and inaccuracy. If an error of the drawings is detected at a later stage the whole process has to start over. The model should be reduced to the minimum required detail as possible. CAD models may be enormous and carry e.g. production information such as holes which can be irrelevant for the FEM simulations. If too much information is put into the model, the simulations time will increase or the mesher may not manage to make a grid.

3. **Predict the results**
   The user should predict the results before starting simulate. By doing so incorrect input data is located easily when postprocessing and incorrect solutions can be avoided. A converged solution does not imply a correct solution.

4. **Construct a mesh**
   Constructing meshes is a laborious process. One may experience converging difficulties when simulating and hence the mesh needs to be adjusted. In order to created proper meshes as efficiently as possible one should start by creating a coarse mesh without any use of extra features. A coarse mesh may not give satisfactory results, but it may give an idea of outcome of the final result. Denser meshes with extra futures may trigger converging difficulties in the simulations. If geometries are symmetric over an arbitrary axis and the medium of interest is assumed to be similar, use of symmetry planes should be applied. This saves simulation time. When simulations are performed without problems the resolution of the mesh shall be increased and extra features appropriate for the case. Checking for grid independency is a common technique to validate a mesh. This is an analysis to check if the solution depends on the grid. If a solution does not vary with the grid configuration the solution is gird independent. Hence further simulations should be executed with the coarsest mesh which is grid independent.

5. **Check the grid**
   Visual and automatic inspection of the grid shall be performed. Neighboring- cells with big aspect ratios and cells with small internal angels may be present and can be visually found. Such cells may cause problems in the simulations. If problematic areas are fixed prior to simulation time will be saved.

6. **Specify the boundaries and material properties**
   The boundaries and the material properties have to be specified.

7. **Pick an appropriate turbulence model for the case (CFD)**
   The choice of turbulence model may influence the final result. In order to check for turbulence model dependency the mesh should be simulated by use of several turbulence models. The deviation between the results should be evaluated in order to pick the appropriate turbulence model for the case. These analyses require small changes by the designer but extensive use of computational power. When time is a limiting factor an extensive turbulence model analysis may be omitted. In this case the choice of turbulence model should be based on prior experience or scientific publications.

8. **Choose an appropriate solver for the case**
   There are many different solvers available. A solver is tailored for specific conditions. The choice of solver shall be based on the conditions for the case.

9. **Start the simulation**
   A case should be simulated until at certain convergence criterion has been obtained. This criterion may vary depending on the accuracy requirement of the simulation.

10. **Evaluate the results**
    Post processing is important. A visual check of the results shall be performed. By doing this it is easier to specify problematic areas and what has to be done to increase the quality of the mesh. For CFD e.g. Y+ values have to be checked. If larger areas where the Y+ vales are not within the range of the turbulence model, the results of the simulations might be poor. For FEM e.g. areas of singularity have to be checked. The results should be compared to laboratory or field measurements for the case or similar cases if possible.

11. **If necessary return to error sources**
    Performing CDF is an iterative process**.** There are always areas which can be further adjusted. One has to know the limit of when to put an end to the process. To obtain satisfactory results requires time and experience.

Appendix E Mechanical robustness of Francis runners, requirements to reduce the risk of cracks in blades

By: Halvard Bjørndal, André P. Reynaud and Anders L. Holo.

This appendix shows the paper in which the laboratory results were mapped onto a FEM – model. Some parts from this thesis have been published in this paper. The paper starts at the next page.

Mechanical robustness of Francis runners, requirements to reduce the risk of cracks in blades

Halvard Bjørndal
Norconsult AS
Vestfjordgaten 4
1338 Sandvika
Norway

André P. Reynaud
Norconsult AS

Anders L. Holo
Norconsult AS

Introduction

There have been an increasing number of failures of Francis runners in Norwegian hydro power plants due to the development of major cracks in the blades after a short time in operation. This problem has occurred both for new turbines and replacement runners. When tendering for new turbines, the owner and consultants have strict evaluation criteria for turbine efficiency and price. However, regarding mechanical robustness, only general design criteria are specified, and these are difficult to quantify. This paper presents some of the major dynamic forces acting on the runner blades. The effect of the dynamic forces on the runner structure will be evaluated against field measurements performed on prototype runners. To conclude this paper, we will discuss some simple criteria that could be included in turbine contracts to ensure the mechanical robustness of new runners.

1. Background

Norconsult is an independent Norwegian multidisciplinary engineering company with large activity in the hydropower industry. Our tasks include assisting hydropower plant owners with development of new projects and solving operational problems. We perform measurements of vibrations, stress and pressure to determine the dynamic behaviour of hydropower units. We have been doing stress measurements during operation on prototype turbine runners since 1997. The measurement method and test equipment are described in /1/. This paper presents results from runners with different head and from different turbine producers to pinpoint general observations related to runner design and operational conditions.

2. Hydraulic loads on the runner

The main hydraulic load on the runner blades is the pressure difference which originates from transformation of flow forces into mechanical shaft torque. The latest design trend has been to increase the pressure gradient near the inlet and reducing it near the trailing edge to reduce cavitation problems. This design also reduces the blade load near the trailing edge. At steady operating conditions, there are also several hydraulic flow instabilities like draft tube surge, rotor stator interaction (RSI), flow instabilities in runner channels, cavitation and vortex shedding.

Draft tube surge, also known as Rheingans whirl, occurs in all Francis units at part load operation, typically at 40-60 % of BEP, and at loads well above Best Efficiency Point (BEP). The pressure fluctuation amplitude depends on the hydraulic interaction between runner and draft tube, and has a frequency of 25-35 % of the runner rotating frequency. Draft tube surge is an operational problem mainly in low head units where the hydraulic impact power from the draft tube is relatively large compared to the turbine power.

Rotor stator interaction is a combination of two phenomena in the space between the guide vane and the runner blades, and has a major influence on high head turbines where the distance between the guide vanes and the runner blades is small. The first phenomenon is the flow disturbance which occurs each time the pressure gradient in front of the runner blade hits the guide vane. The second phenomenon is when the runner blade passes through the guide vane wake as illustrated in figure 1.a. Figure 1.b shows a resulting pressure fluctuation in the vaneless space. There are intensive research activities among major turbine manufacturers to develop representative RSI-models where fluid-structure interaction models are used, one example is /2/.

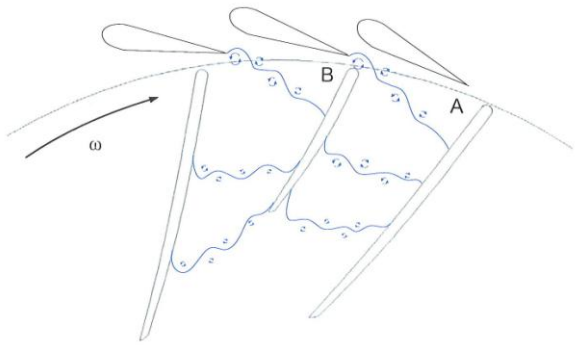

Fig. 1.a Guide vane wake propagation (ref E. Kobro /3/)

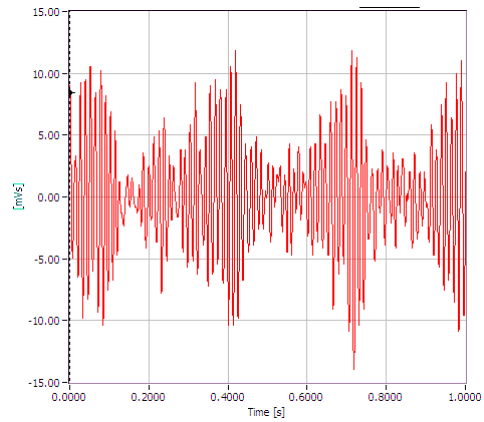

Fig. 1.b Example of measured pressure fluctuation in vaneless space

2. Measured runner stresses

2.1 Stresses in a low head runner

At Frøystul Power Plant in Norway, (P=38 MW, H =54 m, n = 214 rpm), cracks appeared repeatedly at the runner blade trailing edge close to the hub. Measurements with strain gauges were performed during operation /4/ and stresses are shown in figure 2.

At speed no load, the mean stress is dominated by runner centrifugal forces, and the stress variations are moderate. At part load operation, corresponding to a servo stroke between 150 and 310 mm, large stress variations occur with two dominating frequencies. Stress variations at 2-3 Hz occur from Speed-No-Load to 310 mm stroke with a maximum at 245 mm stroke, and are assumed to be related to draft tube surge. From 140 mm to 310 mm stroke additional stress variations are present with a frequency increasing from 25 Hz to 55 Hz, with the maximum amplitude at 190 mm stroke where the frequency was 40 Hz. This is assumed to be related to hydraulic inter-blade vortexes in the runner, as the frequency variation is too large to be related to a mechanical resonance. At 190 mm stroke the 95 % percentile of the peak-peak stress variation was 229 MPa, and a rainflow analysis /5/ of the signals showed 10^4 load cycles per hour with amplitudes larger than 115 MPa. These stress amplitude levels give an unacceptable fatigue loading on the runner, and this explains the problem of cracked blades. Operation around best efficiency point showed low stress variations with no risk of fatigue induced cracking.

Based on these measurements, operation at part load was restricted to only uploading and downloading of the unit. This solved the cracking problem almost completely. It should be noted that this runner does not have an optimal hydraulic design, and similar runners have shown significant smaller stress oscillation at part load.

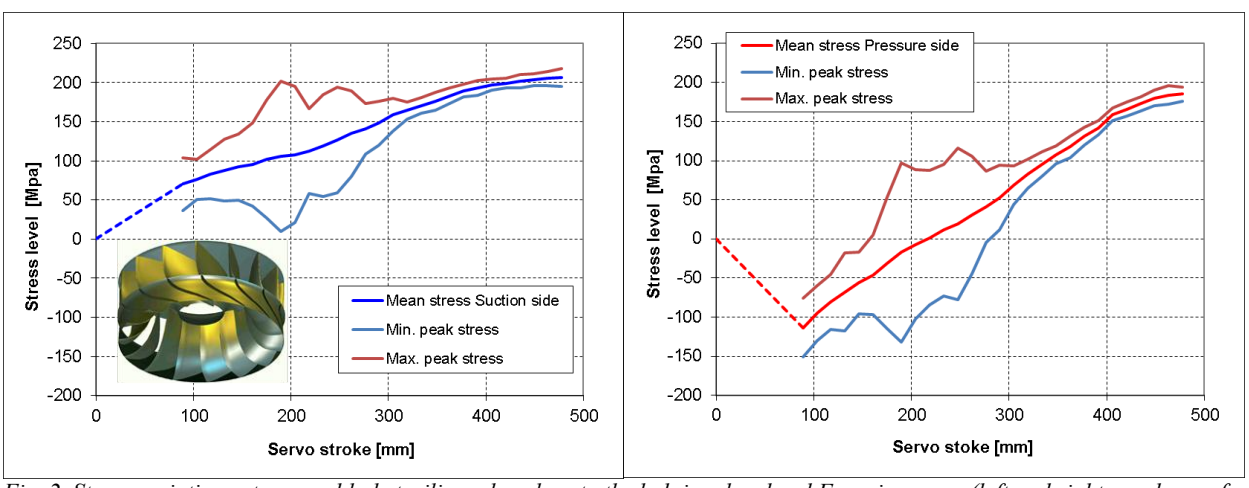

Fig. 2. Stress variations at runner blade trailing edge close to the hub in a low head Francis runner (left and right graphs are for two different measuring points)

2.2 Stresses in a high head runner

We have measured runner stresses in several high head runners with splitter blades and nominal head from 400 to 550 m, and a representative measurement is shown in figure 3. The mean stress level at 100 % servomotor opening is defined to be 1.0 in dimensionless parameters, and the other data is related to this. The stress variations in all the tested units are totally dominated by the guide vane passing frequency caused by guide vane wake propagation through the runner, similar measurement results are reported by H. Brekke /6/. Stress variations at other frequencies have only minor impact in the normal operation range.

The guide vane passing frequency is usually between 150 and 300 Hz. Due to the high frequency of this phenomenon, one of the main design parameters should be resistance to high cycle fatigue. The figure shows how the mean tensile stress increases with load. The stress variations at the guide vane passing frequency are low at Speed-No-Load where the flow is low and the distance between guide vane and runner inlet is at a maximum. With increasing load, the distance between the guide vane and runner inlet is reduced. Combined with a large wake behind the guide vane the maximum stress variations usually occur at between 50 and 60% opening. Operation around the best efficiency point produces the minimum guide vane disturbance (wake) resulting in reduced stress variations even for a short guide vane - runner distance. The distance between guide vane and runner inlet combined with the geometry of the runner blade inlet edge has a large influence on the pressure variations and the resulting stress oscillations. Small changes in the geometry may have a large influence on the stresses in the runner as we have seen on prototypes.

With respect to the fatigue loading, operation at maximum load (above BEP) is the most unfavourable. This is caused by a maximum mean tensile stress combined with high stress variations which gives the maximum stress intensity factor. High residual stress and/or material defects are critical in a high head Francis runner due to the high stress intensity factor and the relatively thin runner blades near the trailing edge. The blade angle and filet radius against the crown and band have significant impacts on the stress concentration and maximum stresses in this area.

Based on these measurements, operating a high head unit at reduced load gives no reduced fatigue lifetime, and thus the unit can be operated from zero to full load without restrictions. It should be noted that operating the unit at overload may be critical related to fatigue since stress variations at a high mean tensile stress increases the stress intensity factor.

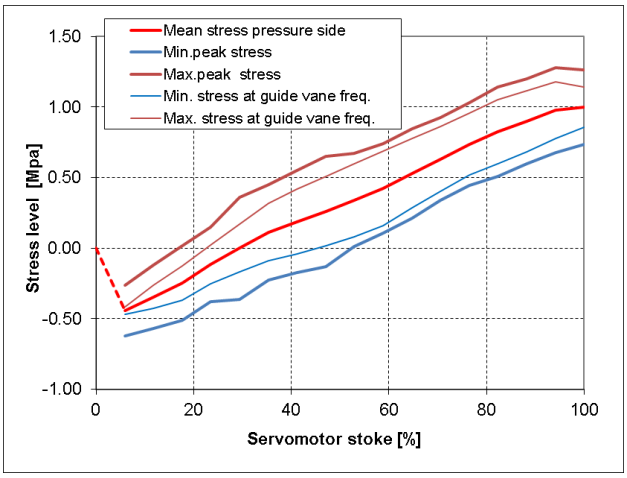

Fig. 3. Stress variations at runner blade trailing edge close to the band (tensile stress is positive) in a high head Francis runner

2.3 Forced response versus resonance induced stresses

The pressure pulsations in the space between the guide vanes and runner are caused by the rotor-stator interaction (RSI). In several Norwegian high head units, hydraulic resonance has occurred due to an unfortunate combination of the number of guide vanes, the number of runner blades, the runner diameter and head cover stiffness leading to pressure wave propagation time between guide vanes equal to the passing period of nearby runner blades. This leads to high amplitude pressure pulsations in the vaneless space. We have inspected runners that have been able to withstand the added dynamic loading without blade cracking, but the resonance caused high noise levels around the turbine.

In high head runners the hydraulic excitation is dominated by the guide vane passing frequency as described above. A mechanical natural frequency of the runner close to the vane passing frequency will result in a resonance that can create large stress amplitudes. To investigate the possibility of a resonance, we have performed tests at part load where the "rough" flow gives stochastic pressure pulsations on the runner blades. Figure 4 shows the results after linear averaging of 300 frequency spectra. The hypothesis is that the stochastic pressure pulsations will excite all frequencies (broadband frequency excitation). If there is a natural frequency present it will appear as a "hill" in the stress frequency spectra due to the amplification factor of the natural frequency. If the broadband excitation has higher intensity in some frequency areas this will give misleading results, but practical experience has shown that the most prominent natural frequencies are detected by this method.

Figure 4 shows four estimated natural frequencies of the runner blade based on this analysis, but the stress amplitudes are very low. The excitation from the guide vane passing frequency (150 Hz) creates a significant forced stress oscillation that is more than a decade higher than the stresses caused by natural frequencies. The first natural frequency at 185 Hz has a separation margin down to the guide vane passing frequency of 23%, which is sufficient to avoid any resonance at nominal speed.
In all the high head runners we have tested, the stress variations have been directly linked to a forced excitation from the pressure variations at the vane passing frequency without any observed amplification from resonating natural frequencies. The presented data indicates that the stress amplitudes in the runner is dependent on the pressure pulsation from the guide vane wake and the runner blade strength – the runner natural frequencies will have no perceptible influence if there is a sufficient separation margin to the major excitation frequencies.

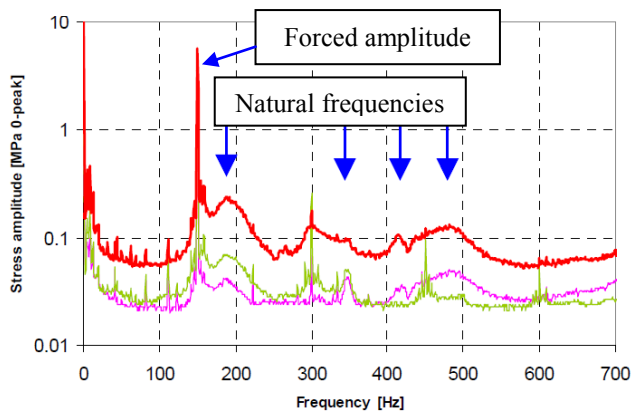

Fig. 4. Stresses from forced response and natural frequencies in a high head runner (The different colours represent different measuring points)

2.2 Additional stresses during Start-up

During start-up, the pressurisation and acceleration of the runner induces large variations in turbine stresses. The number of cycles, however, is very limited - one start/stop per day over 50 years (about 18 000 start-ups) only gives about $1.8 * 10^4$ load cycles. For the mean stress this number of cycles is so low it can normally be neglected when evaluating runner fatigue lifetime.

Strain gauge measurements have shown that the start-up procedure can have significant influence on the runner life expectancy. Traditionally, the guide vanes are opened to a predefined start opening significantly higher than the opening at speed-no load. When the unit speed reaches 90% of nominal speed, the turbine governor adjusts the opening to reach nominal speed. Traditionally, a large start opening was mandatory to give breakaway torque to start the unit before static oil-lift systems in the trust bearing removed the stick-friction. A large start opening gives high water flow into the runner at standstill and when rotating slowly creating significant hydraulic forces acting on the runner blades over a broad frequency range.

Figure 5 shows the resulting stress variations in a high head runner during start-up. The mean stress level at 100% servomotor opening is defined to be 1.0 in dimensionless parameters, and the other data is related to this. Short-Time- Fourier-Analysis was used to investigate the signals in detail. Up to 40% speed, there are broadband stress variations, and only the guide vane passing frequency was easily identifiable. Around 45 % of nominal speed, three times the guide vane passing frequency is identical to a runner blade natural frequency. It seems that this resonance increases the stress variations. At speeds above 45 %, no resonance effects occur, and the flow turbulence intensity is reduced, which reduces the runner stress variations. A rainflow analysis of the 90 second start period gave 75 load

cycles with amplitudes larger than 100 MPa. At one start per day over 50 years the resulting number of load cycles is $1.4 * 10^6$, which will reduce the expected runner lifetime.

We have compared units with different start openings, and our preliminary conclusion is that the start opening should be reduced to make a "softer" start which reduces the runner dynamic loads. Gagnon et.al /7/ has made similar experiments on a low head Francis unit where a reduced guide vane start opening reduced the stress variations. However, reducing the start opening has two possible disadvantages:

- Wear in the bearings increase if the units starts too slowly to build up sufficient oil film, this can however be countered by force feeding oil into the bearings during start-up
- Interference with natural frequencies may give larger number of stress oscillations at high amplitudes even if the maximum amplitude is expected to be reduced due to reduced excitation

Further investigations are needed before a general recommendation can be made.

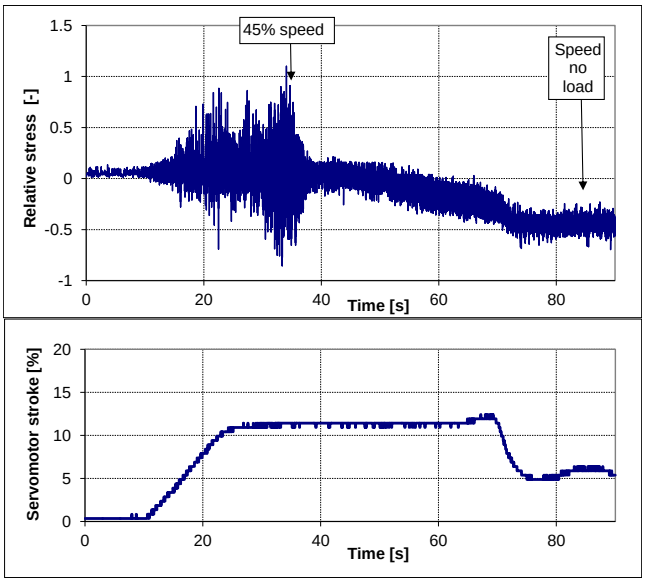

Fig. 5. Stress variations during start-up compared with servomotor stroke in a high head Francis runner

3. FEM calculation based on pressure measurements in a model runner

We have made FEM calculations on a research model runner designed at the Waterpower Laboratory at the Norwegian University of Science and Technology /8/ (open source geometry of a high head Francis runner with splitter blades) where the applied pressures were based on the measurements performed by E. Kobro /3/. This was done to make a qualitative comparison of the effect of static versus dynamic loading in a runner, although the small model runner dimension gives very low stresses compared to a prototype runner.

The calculations were done using ANSYS, where pressures are applied on both the pressure side and suction side of the runner vane. The geometry of the outer parts of the runner (on the outside of ring and hub) has been simplified to reduce the computation time and avoid problematic meshing. The results from the measurements are applied to 8 regions on each side of the runner vane, see figure 6, with the regions between the measurement points subjected to a pressure obtained from a linear interpolation between the two closest measurement points. The static load case is obtained from the average pressures on the runner vane on both pressure and suction sides. The dynamic load case represents the dynamic pressure difference over the runner vane. The amplitude of the dynamic pressure difference is calculated using the difference between the minimum and maximum pressure limits of the 95% confidence interval of the measured pressures (on both sides of the blade); the pressure is assumed to have a normal distribution.

The calculated Von-Mises stresses in the model runner are shown in figure 7. Due to effects linked to the stress direction in the models and the fact that the figure presents Von Mises averaged stresses, the amplitude variation shown is a worst case scenario with the dynamic principal stress directions perfectly aligned with the static principal

stress directions. This should be taken into account when comparing these calculated results to the stress measurements presented in this paper.

Figure 7.a and 7.b have the same colour scale. The maximum calculated dynamic stress was 67% of the maximum static stress (9.3 MPa versus 13.8 MPa) even though the maximum dynamic blade loading was only 28% of the maximum static loading. The reason for this can be seen when comparing figure 6 and 7. The measured dynamic pressures are low over the entire runner blade, but increase near the trailing edge where the runner blade becomes thinner. This results in high stresses at the trailing edge. The static pressure is high at the inlet and drops against the trailing edge, where the runner blade thickness is reduced, which results in a more constant stress loading along the runner blade. It is worth noting that the curved trailing edge of the runner blade makes it more sensitive to dynamic pressure loading compared to a runner with straight cut trailing edge.

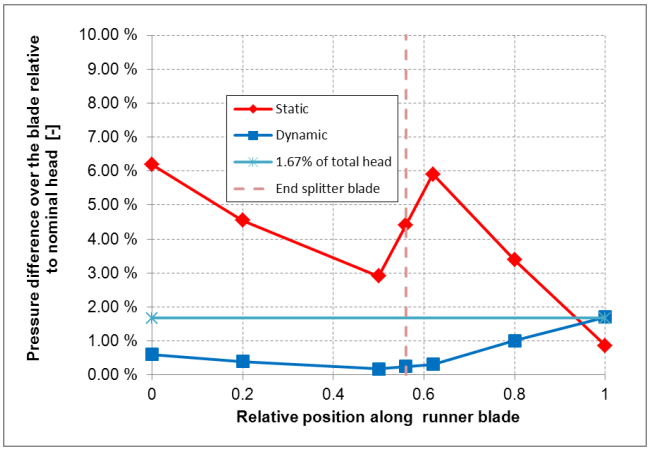

Fig. 6. Applied measured static and dynamic (peak-peak) pressure difference over the runner blade

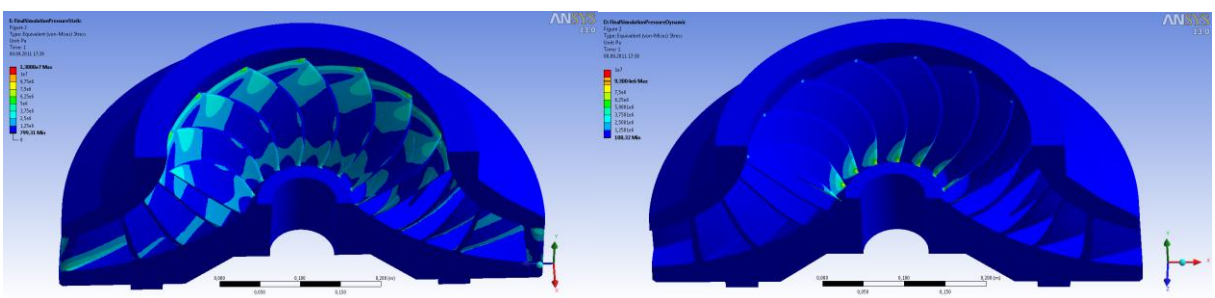

a stress due to measured static pressure load *b Von-Mises stress due to measured dynamic pressure load*

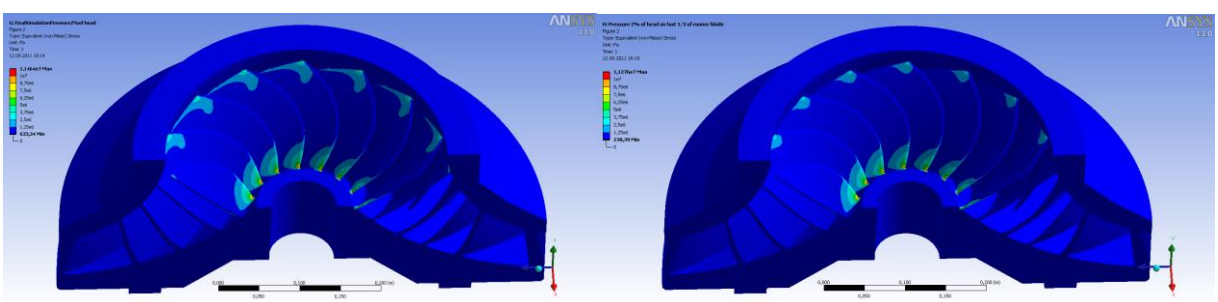

c stress due to 2% of nominal head over runner blade *e Von-Mises stress due to 2% of nominal head over last 1/3rd of runner blade*

Fig. 7. Calculated Von-Mises stresses on a model runner

4. General observations related to turbine design and operation

Over the last 15 years the following trends have been observed:

- Significant reduction of thickness of runner blades, hub and band (runner weight and trailing edge thickness has been reduced)
- Reduced stress concentration due to improved geometry based on FEM calculations
- Turbine geometry is now very close to design geometry thanks to CNC machining
- Material strength remains unchanged
- Better production quality - casting and welding control have been improved (exceptions occur)
- Rougher operating conditions due to more start/stop and operation at part- and maximum- load, less operation at best efficiency point (design load)

One major discussion between plant owner/consultant and turbine manufacturer has been the runner design criteria when using modern CFD and FEM analysis tools.

Traditionally, runner design was based on manual calculations together with extensive empirical formulas that have been developed over many years. Introduction of CFD tools has made large improvements in stationary flow around BEP and is now the basic design tool used by all turbine manufacturers. Calculation of secondary flow and pressure pulsation is subject to extensive research, and is carried out by the R&D department of the turbine manufacturer. Even if some manufacturers have started to implement this in ordinary projects, the CFD calculations at part load remain difficult, and the results are not always trustworthy.
The disagreement starts when it comes to the mechanical design criteria, since there are no standards on how this should be defined. Static loads on the runner blades can be determined by the stationary CFD analysis with high accuracy. The problem occurs when the dynamic loading has to be defined - taking into account all the phenomena described earlier in this paper. We have seen different approaches to the mechanical design related to dynamic loading, especially at the runner blade trailing edge where the dynamic blade loading is stronger than the static blade loading.

Figure 8 shows a dimensionless cross section of 5 different high head runners with similar specific speeds, where different dynamic load criteria combined with different runner design philosophies gave large variations in the trailing edge cross section. Runner 1 was designed by neglecting the dynamic loading, using stationary CFD calculations as the only criteria for the mechanical design optimized by FEM analysis. This resulted in severe blade cracking. Runner 5 is the opposite, where a very conservative approach of the total blade loading has been applied. It should be noted that runner 1, 2 and 3 have all experienced blade cracking.

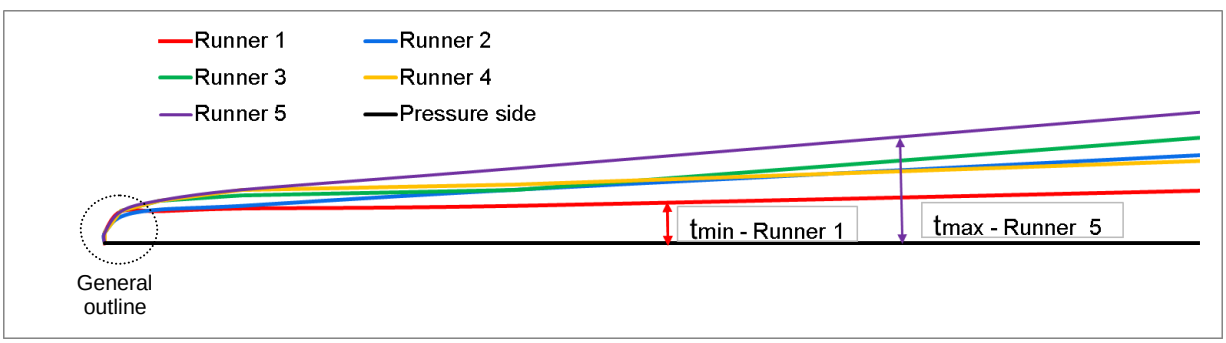

Fig. 8. Dimensionless cross section of 5 different high head runners with similar specific speed

The plant owners should perform an optimization of their production related to inflow variations, regulatory demands and system losses before ordering new units or replacement runners. They have to specify to the turbine manufacturer how they will operate their turbine (regulatory services with operation over the full load range versus operation at BEP only), variations in reservoir and tailwater levels and other requirements. This will give the turbine manufacturer the opportunity to optimize their turbine performance to the plant operational requirements. We have seen far too often that a turbine has been ordered only based on peak efficiency at nominal head and power. This has led to a mismatch between specified and actual operating conditions resulting in unnecessary efficiency losses and other operational problems.

5 Conclusions and recommendations

This paper has investigated many of the dynamic stresses caused by oscillatory flow and resonance phenomena.

Based on these observations some general recommendations can be made:

- Low head Francis turbines experience rough running conditions at part load which increase the dynamic stresses on the runner blades. Minimizing the part load operating time will have a positive impact on the runner fatigue lifetime.
- High head Francis turbines are not subjected to the same increased stresses at low loads, and can normally be operated over the entire load range, except for a narrow load range where the draft tube surge is significant. At overload the combination of higher mean tensile stress and dynamic stress amplitude will have a negative impact on runner fatigue lifetime.
- Thicker runner blade outlet will give increased mechanical strength and will reduce the stress oscillation amplitude. This increases the runner fatigue lifetime and reduces the risk of blade cracking.
- Reducing the guide vane start opening will reduce high stress amplitude cycles during acceleration of the runner to nominal speed. This is especially important for units with many start/stop.

Experience from many plants and investigations presented in this paper shows that dynamic loading in the runner is a major source of runner blade cracking. Designing runners only based on static CFD and FEM calculations is insufficient; added strength to withstand dynamic loading has to be included in the design.

The hydropower industry have today no precise dynamic load criteria that could be used in turbine contracts to ensure the mechanical strength of new runners. As a temporary solution, the manufacturer should document the expected dynamic load on the runner based on advanced studies and measurements, or as a minimum perform FEM analysis of the runner using a part of the static head as load on one side of the blade.

References

1. Bjørndal H, Moltubakk T, Aunemo H 2001 "Flow induced stresses in a medium head Francis runner - Strain gauge measurements in an operating plant and comparison with Finite Element Analysis" *Proc. of 10th International Meeting of the IAHR Work Group on the Behaviour of Hydraulic Machinery under Steady Oscillatory Conditions (Trondheim, Norway)*
2. Yan J, Koutnik J, Seidel U, Hübner B "Compressible simulation of rotor-stator interaction in pump-turbines" *25th IAHR Symposium on Hydraulic Machinery and Systems (Timisoara, Romania)*
3. Kobro E 2010 "Measurements of Pressure Pulsations in Francis Turbine" Doctoral thesis at NTNU, 2010:136 *ISBN 978-82-471-2239-6*
4. Bjørndal H 2002 "Frøystul Power station – Stress measurement on turbine runner during operation (in Norwegian)" appendix 3 in Start-stop costs for hydro power units, Technical and financial consequences *Energi Norge publication ISBN 82-436-0453-7*
5. ASTM Designation E1049-85(1990): "Standard Practice for Cycle Counting in Fatigue Analysis"
6. Brekke, H 2009 "Life time and safety of hydro turbines" *HYDRO 2009, (Lyon, France)*
7. Gagnon M, Tahan S A, Bocher P, Thibault D 2010 "Impact of startup scheme on Francis runner life expectancy" *25th IAHR Symposium on Hydraulic Machinery and Systems (Timisoara, Romania)*
8. Not published, model runner geometry free available from the Waterpower Laboratory at the Norwegian University of Science and Technology, Trondheim, Norway

The Authors

Halvard Bjørndal Master degree in mechanical engineering from the Norwegian University of Science and Technology, Norway 1990. Vice president and Head of mechanical section of the Energy division in Norconsult. Extensive experience from plant commissioning, advanced field measurements and condition analysis of hydropower units, process pumps, gas turbine packages, centrifugal gas compressors, ship propulsion systems and hydraulic control systems.

André P. Reynaud graduated in Génie Mathématique et Modélisation from the Institut National des Sciences Appliquées de Toulouse, France in 1998. He has headed the Measurement and Analysis Group of the Mechanical section of the Energy division in Norconsult since 2008. His working experience includes vibration measurements and analysis on more than 30 hydropower units as well as advanced dynamic analysis of structures calibrated with measurements.

Anders L. Holo has participated in the research for this paper during his summer internship at Norconsult AS. He is currently a student at NTNU completing his Msc. thesis work, the thesis work is directly linked to the FEM calculation performed in this paper.